UNIVERSITY OF OKLAHOMA

GRADUATE COLLEGE

CONTROLS OF PRE-EXISTING NORMAL FAULTS ON THE GEOMETRY AND LOCATION OF THRUST FAULTS IN FOLD-THRUST BELTS

A THESIS

SUBMITTED TO THE GRADUATE FACULTY

in partial fulfillment of the requirements for the

Degree of

MASTER OF SCIENCE

By

SHIVA BASNET
Norman, Oklahoma
2016

CONTROLS OF PRE-EXISTING NORMAL FAULTS ON THE GEOMETRY AND

LOCATION OF THRUST FAULTS IN FOLD-THRUST BELTS

A THESIS APPROVED FOR THE
CONOCOPHILLIPS SCHOOL OF GEOLOGY AND GEOPHYSICS

BY

_____
Dr. Shankar Mitra, Chair

_____
Dr. Kurt Marfurt

_____
Dr. Ze'ev Reches

This work is dedicated to my family and close friends.

Acknowledgements

First and foremost, my most sincere thanks to my advisor, Dr. Shankar Mitra for leading me into the world of analog modeling. Truly speaking, only with his continuous guidance, constant support and encouragement was I able to dive into the depths of this research, understand everything, and arrive at the end successfully. I would also like to extend my heartfelt gratitude to Robert Turner for cutting the wood blocks into desired angles. Without his help, I would have not been able to work at the desired setting, pace, and comfort at which I have been working. A Special thanks to Dr. Kurt Marfurt and Dr. Ze'ev Reches for their invaluable discussion on the subject. I would like to thank all professors and graduate students from the ConocoPhillips School of Geology and Geophysics, especially Simon Zu, Benmadi Milad, and Jianjun Li for their support. I also appreciate the Surfer © for the computer software which was a great help in collaborating this project. A very special thank you goes to my wonderful wife, Nirmala, and son, Shreesh for all their love, support and patience. Sincere gratitude goes out to my parents for their encouragement and support throughout my academic career. Golden Software deserves another huge thank you for Surfer trial version, which made the analysis and processing of the data easier on my own computer. Finally, special recognition should be given to CPSGG for funding and Scholarships.

Table of Contents

List of Figures

Abstract

Pre-existing normal faults are commonly cited as influencing both the sequence of faulting and the location of thrust faults in fold-thrust belts. Scaled experimental models for both frictional and ductile detachments were conducted to study the influence of pre-existing normal faults on the subsequent development of thrust faults. Frictional detachment experiments used layers of silica sand directly overlying the detachment, whereas ductile detachment experiments used layers of sand representing sediments overlying silicone gel, representing a ductile layer in 60° angle normal faults. The experiments suggest that the normal faults influence the location and orientation of the frontal thrusts rather than the sequence of fault propagation. Furthermore, the influence is more pronounced for detachment folds and thrusts formed above a ductile detachment than for duplexes above a frictional detachment. The orientation of the normal faults influences the orientation of subsequently formed thrust faults in different ramp settings, so that normal faults with orientations oblique to the direction of contraction result in oblique frontal thrusts. Offsets in the location of the normal faults along lateral ramps or transfer zones result in offsets in the location of the frontal thrusts. The effect of the pre-existing normal faults on the thrust-fold geometry depends on the relative distance between the normal fault and the forethrust positions, detachment type, and the geometry of the normal fault. The results are directly applicable for understanding the locations and orientation of thrust faults, mapping of fold-thrust structures using surface and subsurface data, and for comparison with natural examples.

1 Introduction

1.1 Introduction

The formation of the sedimentary basins is commonly associated with the formation of normal faults, resulting in symmetric grabens or asymmetric half-grabens. Contraction induced by tectonic or gravitational forces results in reverse faults and the interaction between these faults and the pre-existing extensional structures occurs during the closure of the basin. Three main types of interactions occur between compressional structures and pre-existing normal faults [*Mitra*, 1993] (Figure 1.1): (1) the normal faults can be reactivated as reverse faults resulting in the formation of inversion structures, (2) the normal faults can act as buttresses and provide stress concentrations for the localization of thrust faults, and (3) the normal faults can be folded and decapitated by the reverse or thrust faults.

In this thesis, I address the geometry and kinematic evolution of fold and thrust structures formed by the buttressing effect of pre-existing normal faults. A normal fault, which offsets a stiff stratigraphic unit, provides a mechanical perturbation and hinders the propagation of the fold and thrust belt towards the foreland [*Mitra*, 1988; *Butler*, 1989; *Sassi et al.*, 1993; *Tavarnelli*, 1996]. Further contraction at the perturbation results in a fault-related fold whose forelimb and backlimb may cut by thrust ramps branching off the basal detachment. The normal fault is eventually truncated or thrusted over, and the compression front migrates toward the foreland.

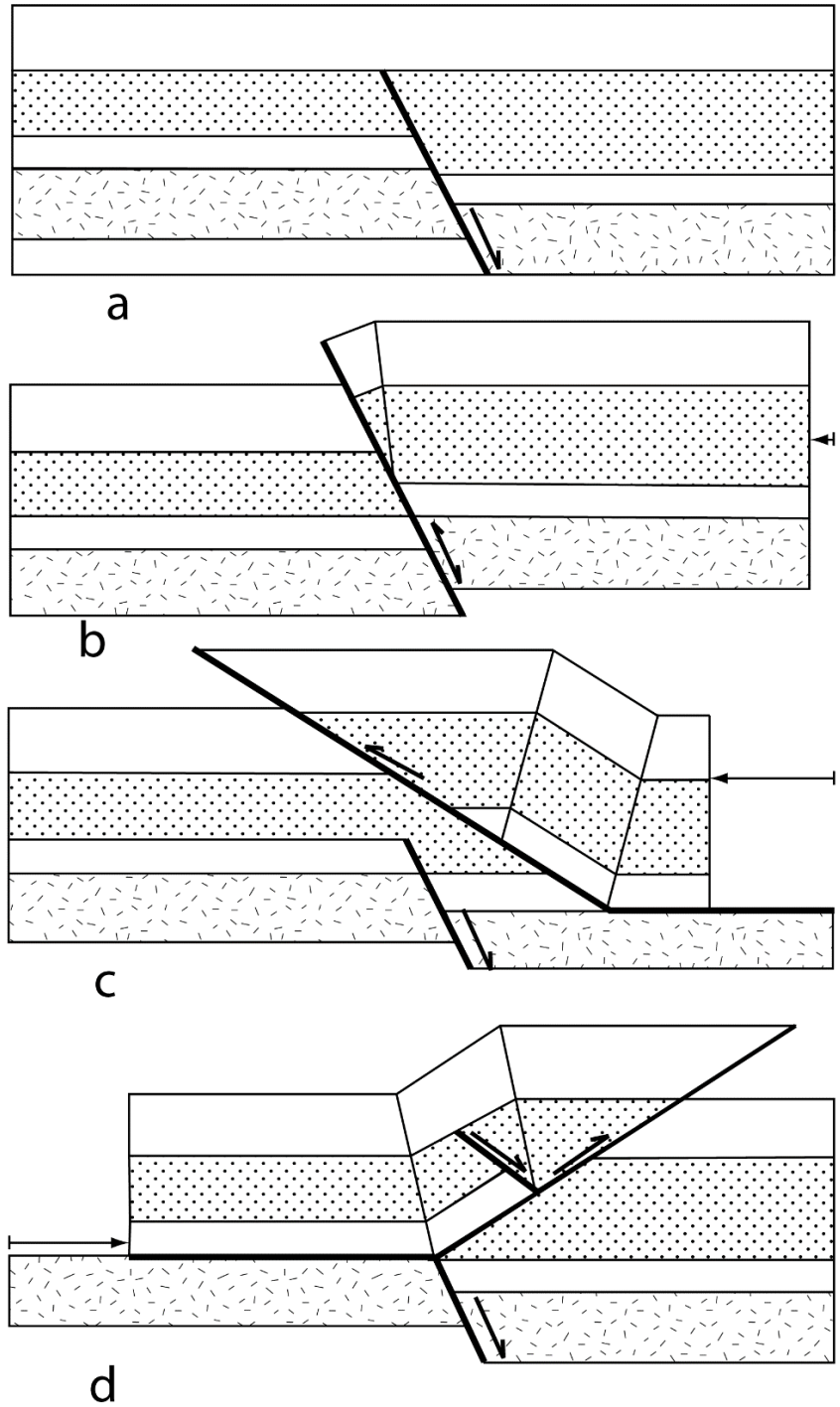

Figure 1.1 Three main types of interactions between compressional structures and pre-existing extensional structures: (a) planar normal fault, with synextensional units (stippled pattern) thickening in the hanging wall; (b) normal fault reactivated as as reverse fault resulting in an inversion structure; (c) normal fault providing a stress concentration for the localization of thrust faults; (d) normal fault folded and decapitated by later-formed compressional structure. Arrows in b-d indicate the direction of compression [*Mitra*, 1993].

Both the sequence of thrust formation and the location of thrust faults may be influenced by the presence of pre-existing normal faults. Furthermore, their geometries and trends may be influenced by the normal faults. Therefore, a detailed analysis of the different types of structures formed above normal faults during contraction is useful for interpretation of fold-thrust structures.

This study investigates the role of the pre-existing normal faults on fold-thrust geometries developed above both ductile and brittle detachments using scaled sandbox experiments with different normal fault geometries. The models are compared with examples of natural fold-thrust belt structures that are influenced by pre-existing normal faults.

1.2 Objectives

The main objective of the current study is to analyze the influence of pre-existing normal faults on the geometry and kinematics of the fold-thrust structures using scaled sandbox models. The study considers structures formed above the two types of basal detachments: (a) brittle (sand), and (b) ductile (silicone gel), and investigates a number of normal fault settings, including frontal, lateral, and oblique, and more complex settings, including offset, oblique intersecting, and curved ramp settings (Figure 2.1). This analysis mainly emphases on the evolution and geometry of the frontal thrust and associated folds developed above the normal faults. Moreover, quantitative analysis of the wedge height, fault spacing, fault dip, and the position of the frontal thrust relative to the top of the normal fault are interpreted using cross sections, progressively deformed top images, and 3-D laser scanning data. The model results are compared

with natural fold-thrust belts with pre-existing normal faults. These models may be useful to interpreting the subsurface structures using surface and subsurface data.

1.3 Previous studies

The geometry, kinematics, and dynamics of the fold-thrust belts could be related to many parameters such as lithology of the deforming crust, decollement dip, pre-existing extensional structures such as normal fault, tectonic underplating, basal friction, oblique convergence, and surface processes such as erosion [*Schreurs et al.*, 2006; *Nilforoushan et al.*, 2008]. There have been many comprehensive studies that focused on the effects of brittle and ductile detachments on the propagation, topography, geometry, and strain in fold-thrust belts [e.g., *Davis and Engelder*, 1985; *Cobbold et al.*, 1989; *Costa and Vendeville*, 2002; *Bahroudi and Koyi*, 2003]. Thrust front reaches farther in area detached on a ductile detachment whereas above a brittle detachment area shortening is accommodated by additional uplift and penetrative strain [*Cotton and Koyi*, 2000].

A role of pre-existing normal faults on fold-thrust development is observed in several fold-thrust belts including southwestern Appalachian, Alps, Alberta Foothills, and Potwar Salt Range Province. *Sassi et al.* [1993] investigated the mechanical role of the pre-existing faults in thrusting along a detachment using analog and numerical models. The pre-existing faults resulted disturbed dilated zones with 10-20 % lower friction angle than the homogeneous sand. In the thrust systems, reactivation of the faults depends on their orientations to the stress field and spacing of the pre-existing faults. [*Cotton and Koyi*, 2000] used sand as the frontal ramp to show the deformation style above a ductile and a frictional detachment. *Dixon and Spratt* [2004] used centrifuge models to explain the effect of lateral ramp and tear faults in the Limestone Mountain

area of the southern Alberta Foothills thrust system. They found a transverse link between two frontal ramps is unstable and the transverse link is abandoned to form a transfer zone. *Faisal and Dixon* [2015] also used a centrifuge analog models to investigate the structure differences in the frontal and the lateral ramp settings and compared those structural variations along and across strike structures in the Salt Range and Potwar Plateau.

Kinematic models that show the influence of pre-existing normal fault on thrust ramp development are explained by *Mitra* [1993] (Figure 1.1) and *Tavarnelli* [1996]. Restored balance sections are used to explain the role of pre-existing normal fault in detachment thrusting in Southwestern Appalachian [*Mitra*, 1988],Western Alps [*Butler*, 1989], and Umbria-Marche Apennines [*Tavarnelli*, 1996]. Buttressing effect of the normal fault can result in localization of thrust, upright folds, strain, and cleavage intensification in the thrust belts [*Butler*, 1989].

Inversion structures kinematics and geometries formed by the compressional reactivation of pre-existing normal fault are well documented in detail [*Glennie and Boegner*, 1981; *McClay*, 1989; *Mitra*, 1993; *Mitra and Islam*, 1994]. In previous studies, the importance of the pre-existing normal faults without undergoing reactivation in fold-thrust geometries has been noticed, however, the detail investigations of the fold-thrust geometries detached on brittle and ductile detachments in different normal fault settings using analog modeling with detail interpretation are scarce.

2 Methodology

Analog models are scaled experiments that use low strength materials such as sand, clay, wax, silicone putty, and beads to simulate tectonic processes [*Hubbert*, 1937; *Koyi and Mancktelow*, 2001]. Geological data from many fold and thrust belts suggest that the structural inheritance in the form of a various type of heterogeneities such as pre-existing arrays of faults, decollement horizons due to ductile materials (clay-evaporites), and stratigraphy pinchout have important implications for the fold and thrust structures [*Butler*, 1989; *Jean Letouzey*, 1990]. In this study, two sets of experiments for brittle (sand) and ductile (silicone gel) detachments were conducted with pre-existing normal faults acting as buttresses that influence the development of thrust faults. The fold and thrust geometries in two different detachment sets are compared to investigate the role of the normal fault for different normal fault settings. The primary questions addressed were: (1) the role of the normal faults in influencing the geometry and location of the thrust faults; (2) the difference in the influence for ductile and brittle detachments, and (3) whether the normal faults influence the sequence of development of the thrust faults.

2.1 Set up of the sandbox experiment

A sandbox of 57 cm X 33 cm X 15 cm was used for the experiments. Wood and steel blocks pre-cut into different configurations have been used in the past to represent basement faults for analog experiments [*Sanford*, 1959; *Lowell*, 1970; *Horsfield*, 1977; *Groshong and Rodgers*, 1978; *Tsuneishi*, 1978; *Withjack et al.*, 1990; *Bose and Mitra*, 2009]. In the current study, pre-existing normal faults were simulated with a wood block 0.7 cm thick pre-cut so as to form a fault dipping 60° towards the hinterland.

Eleven different sets of experiments were done that included both brittle and ductile detachments, including: (1) a single frontal ramp: model BDFR and model DDFR, (2) a frontal ramp offset along a vertical transverse fault: model BDOFR and model DDOFR, (3) an oblique ramp trending degrees: model BDOBR and model DDOBR, (4) a frontal ramp bounded by a vertical lateral ramp: model BDLR, and model DDLR, (5) two frontal ramps with an oblique intersection: model BDOBIR, and (6) a curved frontal ramp: model BDCR and model DDCR (Figure 2.1). These configurations were chosen because they represent some of the common possibilities in natural structures. The basin formed on the downthrown side of the pre-existing normal fault was filled up to the top of the normal fault (wood block) with sand or sand overlying silicone gel to represent brittle and ductile detachments, respectively. Loose sand was sieved and distributed uniformly into the box to form a total thickness of about 3 cm above the top of the wood block to represent the sedimentary cover (Figure 2.2).

A motorized backstop shortened the section with the constant speed of 1.5 cm/hour for 6 hours for a net shortening of 9 cm. The models were illuminated oblique to the contraction direction to differentiate foreland and hinterland dipping thrusts. Sequential top photograph images were taken at regular intervals using a digital camera mounted above the sandbox to capture the progressive deformation. Uniform 0.5-inch-wide square grids imprinted on the top of the model enabled tracking of the deformation. After each hour of shortening, the experiment was stopped for a short time to scan the 3-D model topography. After completion of the experiment, the models were covered with loose sand and saturated with water to cut cross-sections parallel to the contraction direction. Rigid side walls resulted in edge effects along the margins. Therefore, the top

images were trimmed off on the margins to remove edge effects. The interpretation of the main structures in the center of the model was not affected by the edge effects.

2.2 Material properties and scaling

This study used fine-grained sand ranged from 0.15 - 0.2 mm. The geometry of the sand wedge and the kinematics of the internal structure are controlled by the internal friction and cohesion. It also depends on the detaching layer whether brittle or ductile, detachment thickness, cover sediment compaction, an overburden thickness, basal friction between the material and the pre-existing fault or discontinuities. The cover sediments on the top of the basal detachments (sand for brittle frictional detachment and silicone gel for ductile detachment) was 3 cm thick dry quartz sand, a Mohr-Coulomb material with negligible cohesion. Silicone gel, a Newtonian viscous fluid, (from Crazy Aaron Enterprises ©) [*Karama*, 2014] used had a viscosity of 10.1 X 10^4 Pas and density of 0.9 g/cc and represents the salt. The experimental material properties, geometry, and kinematics such as density, viscosity and strain require proper scaling [*Hubbert*, 1937; *Weijermars and Schmeling*, 1986]. The model settings had a geometric scaling of 10^5 i.e. 1 cm in the model corresponding to 1 km in nature. In regard to time, each hour of shortening in the experiment corresponded to 1 million years in nature. To distinguish between two interlayers white sand was colored with dark gray which did not modify the bulk material properties significantly. The pre-existing normal fault was simulated by a wood block of 0.7 cm thick pre-cut at about 60° dip dipping towards the hinterland. The wood block is rigid and act as buttress and controls the geometries of the thrusts and prevents the detachment deformation beyond it toward the foreland in the current experiment setups.

2.3 Model Interpretation

The progressive deformation in each model was interpreted using sequential top photos. In experiments involving brittle detachments, imbricate thrusts formed with a high taper angle [*Letouzey et al.*, 1995] and greater relief. The frontal structure verged toward the foreland, whereas in the ductile detachment experiments asymmetric detachment folds formed in the hinterland, and more symmetrical frontal pop-up structures grew coevally with a low taper angle in the foreland. The detachment folds were faulted during further contraction. The frontal ramp created a foreland verging fault-related fold. The normal fault influenced the location and geometry of the frontal thrust but not the sequence of faulting. The frontal thrust orientated oblique to the contraction direction results in oblique thrust fault. Offset and lateral ramp settings result in two variable propagating frontal wedges connected with the transfer zone [*Dixon and Spratt*, 2004]. Transverse structures connecting the two wedges were rotated and eventually become unstable.

Cross-sections were used to measure the fault dip, distance from the top of the normal fault to the base of the forethrusts, and to interpret the lateral and vertical propagation of the structures. In addition to thrust geometries, cross-sections of the ductile detachment models were used to map the silicone distribution. 3-D laser scanning data were used to create the topography and profiles of the deformed models.

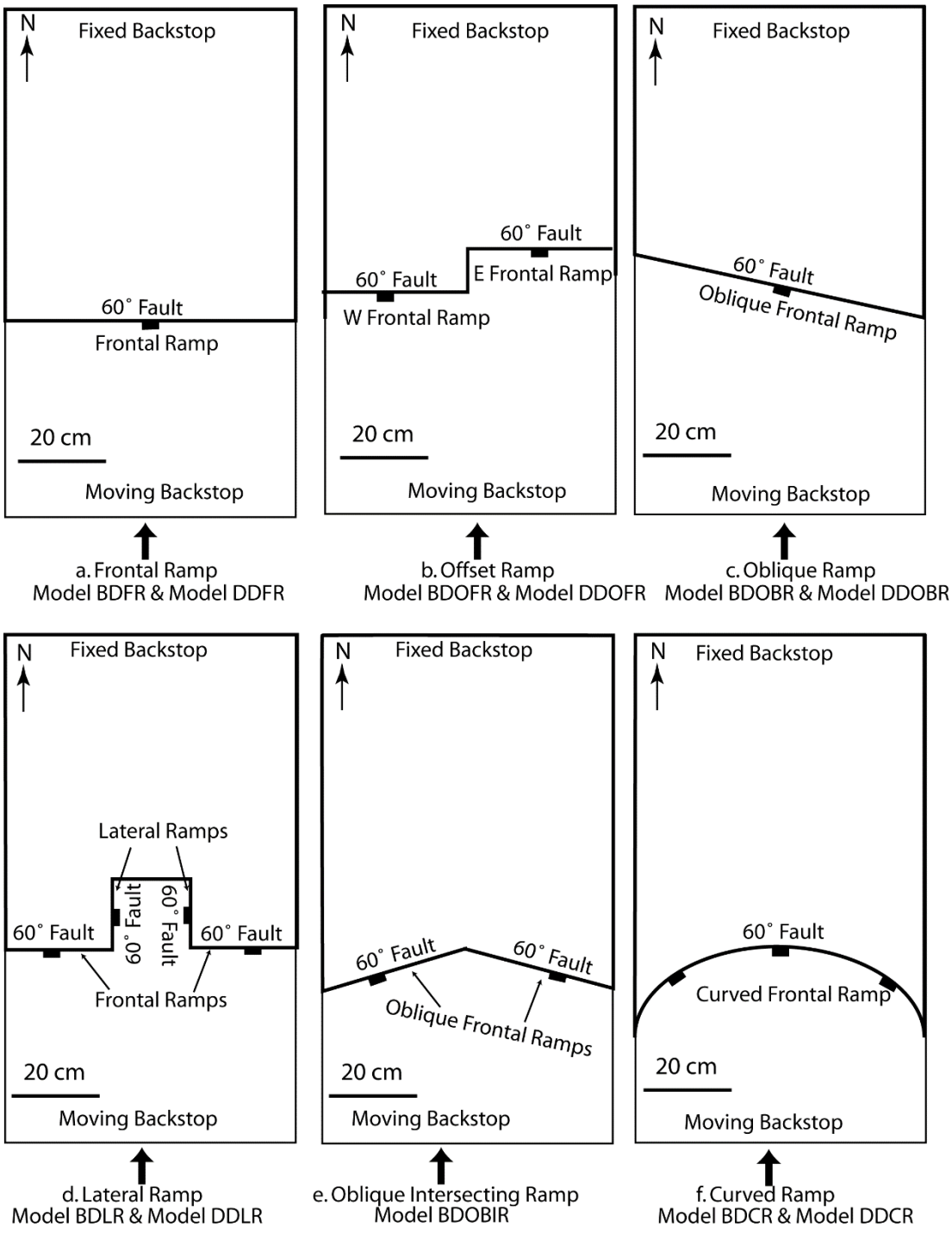

Figure 2.1 Plan view of the experiments showing the position of the pre-existing normal faults. Basin south of normal faults was filled with sand (brittle) or silica gel (ductile) detachment up to the level of the top of the normal fault (wood) which was further covered with 3 cm sand and compressed from south to north. (a) A frontal ramp; (b) a frontal ramp offset along a vertical transverse fault; (c) an oblique ramp trending 76 degrees; (d) a frontal ramp bounded by a vertical lateral ramp; (e) oblique intersecting frontal ramps; and (f) a curved frontal ramp.

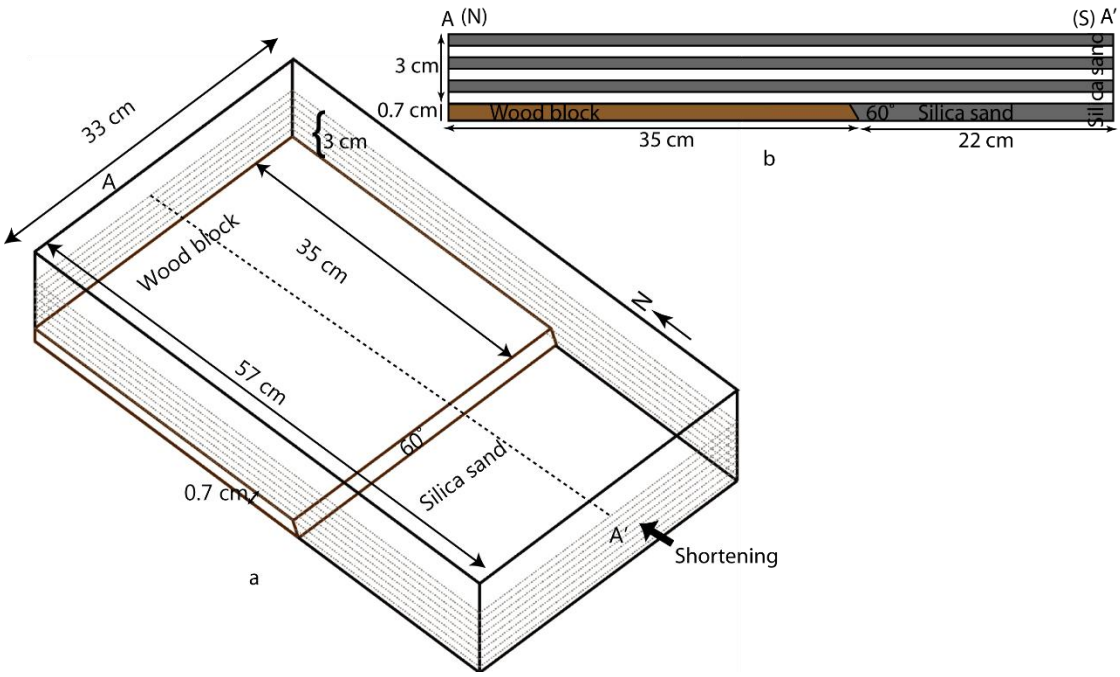

Figure 2.2 Frontal ramp brittle detachment experiment set up (Model BDFR) (Fig. 2.1a). (a) 3-D view; (b) cross-section A-A'. In all experiments, shortening was from South to North.

3 Results

All models were deformed at a rate of 1.5 cm/hour for 6 hours to obtain a total shortening of 9 cm. Three different top view photos of deformed sand models at 3, 6, and 9 cm are shown for all experiments. For reference, the north direction has been placed horizontally to the right of the page. In all models, the contraction was applied from the south (left) to the north (right) (Figure 3.1). All the sections were orthogonal to the shortening direction (north-south) and were facing the east. The height of the wedge was measured above the top of the initial undeformed sand. Baseline kinematics and deformation mechanisms for the formation of the foreland verging imbricate thrusts and duplexes in the brittle detachment, and the development of symmetric to asymmetric detachment fold, pop-up, and pop-down structures are explained, respectively in the brittle (model BDFR) and ductile (model DDFR) detachments on the frontal ramp experiments. In other complex ramp experiments, only the main differences in the structures and geometries of the fold-thrust belt between different ramp settings and among two types of detachments brittle and ductile are discussed.

3.1 Model BDFR: Brittle detachment on a frontal ramp

Foreland verging duplexes consisting of five imbricate thrust sheets (T1-T5) were formed (Figure 3.1) which were transported into the foreland as piggyback stacks. The deformation started with a foreland verging fold where a forethrust developed connecting inflection points on the beds. The deformation in the hinterland was controlled dominantly by a backthrust BT1 formed near the backstop. The strain was dissipated in thickening of the wedge and foreland propagation of forethrusts (Figure

3.2). The map view of the frontal thrust, T5, followed the geometry of the frontal ramp of the pre-existing normal fault. T5 first formed parallel to the normal fault and then stepped over it (Figure 3.1c & Figure 3.2). The forethrusts (T1-T4) progressively increased dips from 24° to 34°, as they were rotated and carried by the younger forethrusts toward the foreland (Figure 3.2). Fault spacing between thrusts T1-T2 and T3-T2 was 1.6 cm, T3-T4 was 2.4 cm and T4-T5 was 6 cm (Figure 3.3). Frontal thrust T5 formed at a greater fault spacing than its predecessor forethrusts (T1-T4), due to the presence of a pre-existing normal fault as the frontal ramp. Therefore, the normal fault ramp influenced the location of the frontal thrust fault, but not the sequence of faulting.

Backthrust BT2 developed due to the buttressing effect of the frontal ramp and to accommodate the deformation from the frontal thrust T5. In the final stage, the height of the wedge was 3.7 cm above the initial top sand (Figure 3.3). The frontal thrust, T5, formed 1.7 cm from the normal fault. This model BDFR is the prototype model which shows the baseline kinematic and geometries of the fold and thrust belts for the brittle detachment and serves as a comparison for subsequent more complex normal fault geometries for brittle detachments.

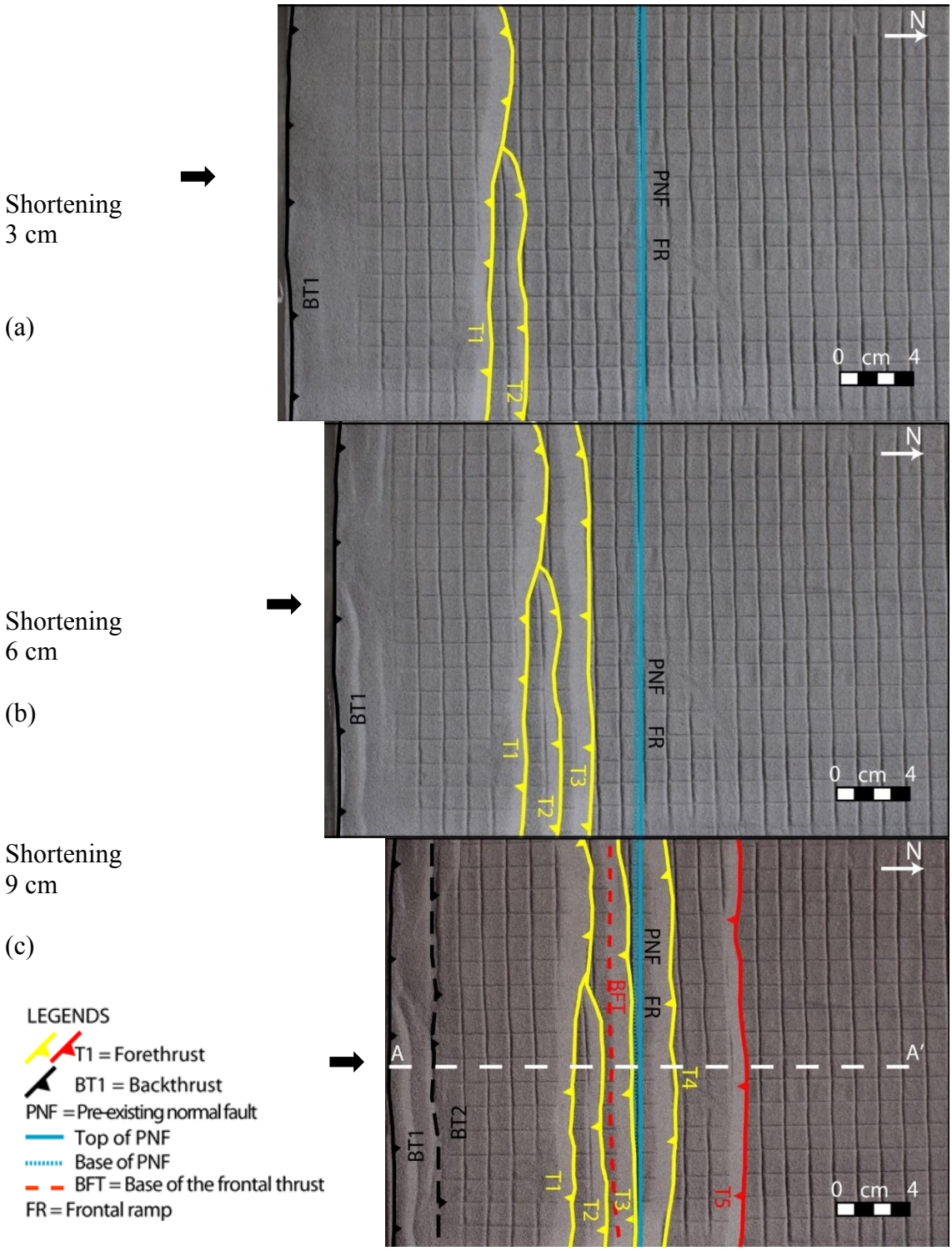

Figure 3.1 Progressive top photos of the brittle detachment on a frontal ramp experiment, model BDFR, with fault interpretation. (a) 3 cm shortening; (b) 6 cm shortening; (c) 9 cm shortening. A-A' shows the cross-section line for Figure 3.2.

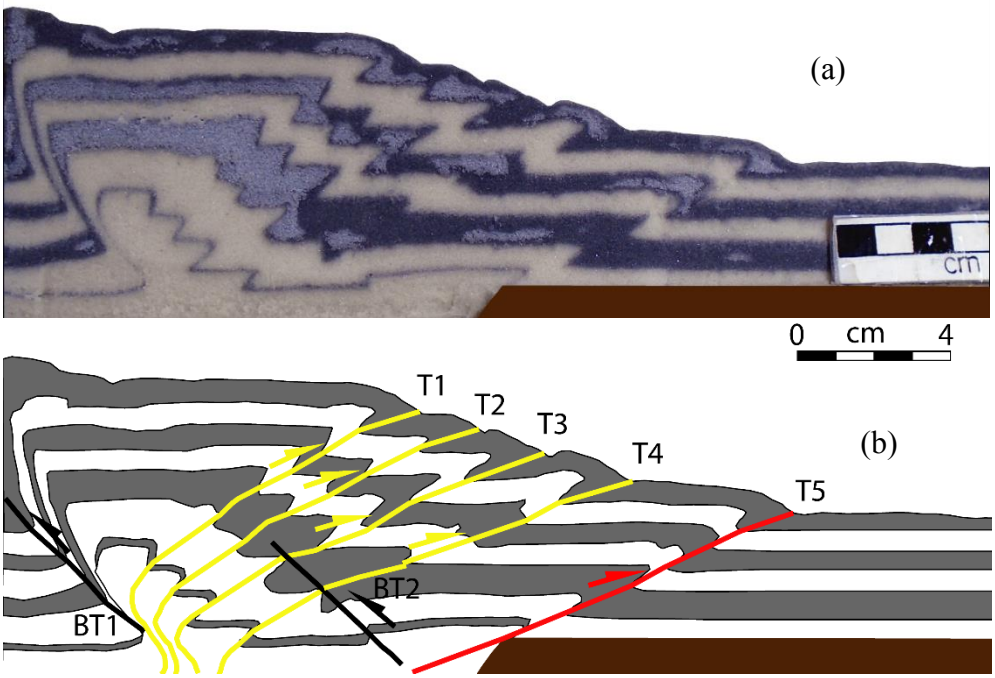

Figure 3.2 Section A-A' of a brittle detachment on a frontal ramp experiment model BDFR (see Figure 3.1 for location). Foreland verging imbricate forethrusts showed a systematic decrease in dips in the direction of transport in a piggyback thrusting sequence. BT1 = backthrust, T1-T5 = forethrusts younging in age. (a) Section image; (b) line drawing of a section A-A' with fault interpretation.

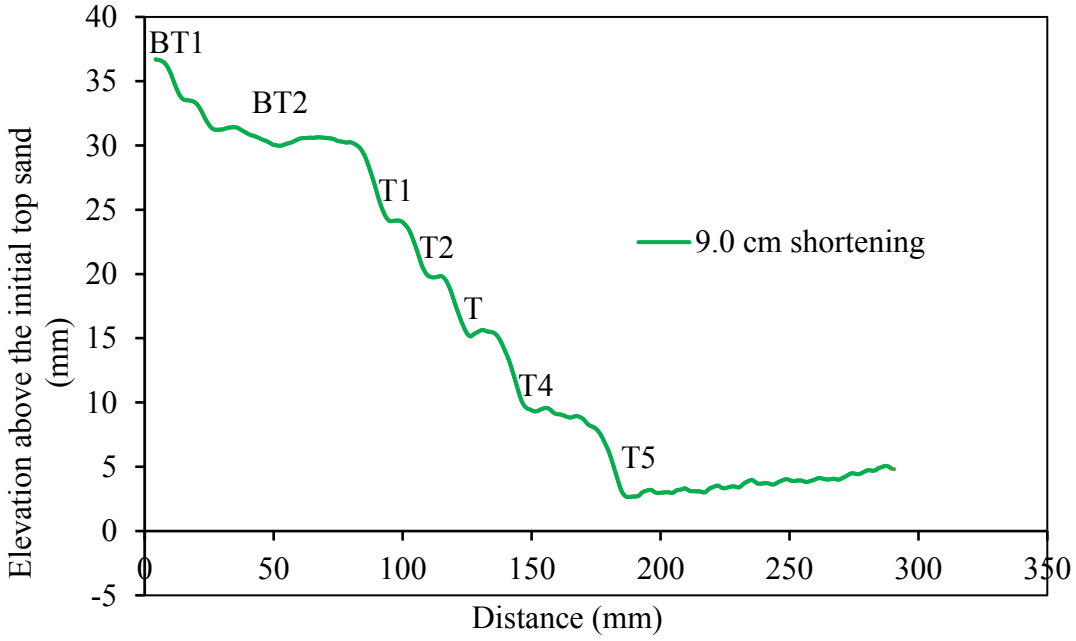

Figure 3.3 Final top surface profile along A-A' of the brittle detachment on a frontal ramp experiment, model BDFR, (Figure 3.1) after 9 cm shortening. Elevations are above the initial undeformed sand top (0 cm shortening).

3.2 Model DDFR: Ductile detachment on a frontal ramp

The deformation started with a formation of a backthrust and related faulted detachment fold, followed by a forethrust and a similar related structure. Both structures were asymmetric and were associated with back thrusts. (Figure 3.4). The structures became tighter with increasing deformation with the silicone gel flowing into the cores of the folds. The backthrusts and forethrusts rooted in the basal silicone layer. The frontal thrust, T3, climbed the frontal ramp of the normal fault and onto the upper flat (Figure 3.4 & Figure 3.5).

In this model, the deformation front traveled 8.7 cm toward the foreland from the top of the normal fault. Propagation of the frontal thrust toward the foreland was farther in this model DDFR compared to the model BDFR; however, the wedge height was less than in model BDFR.

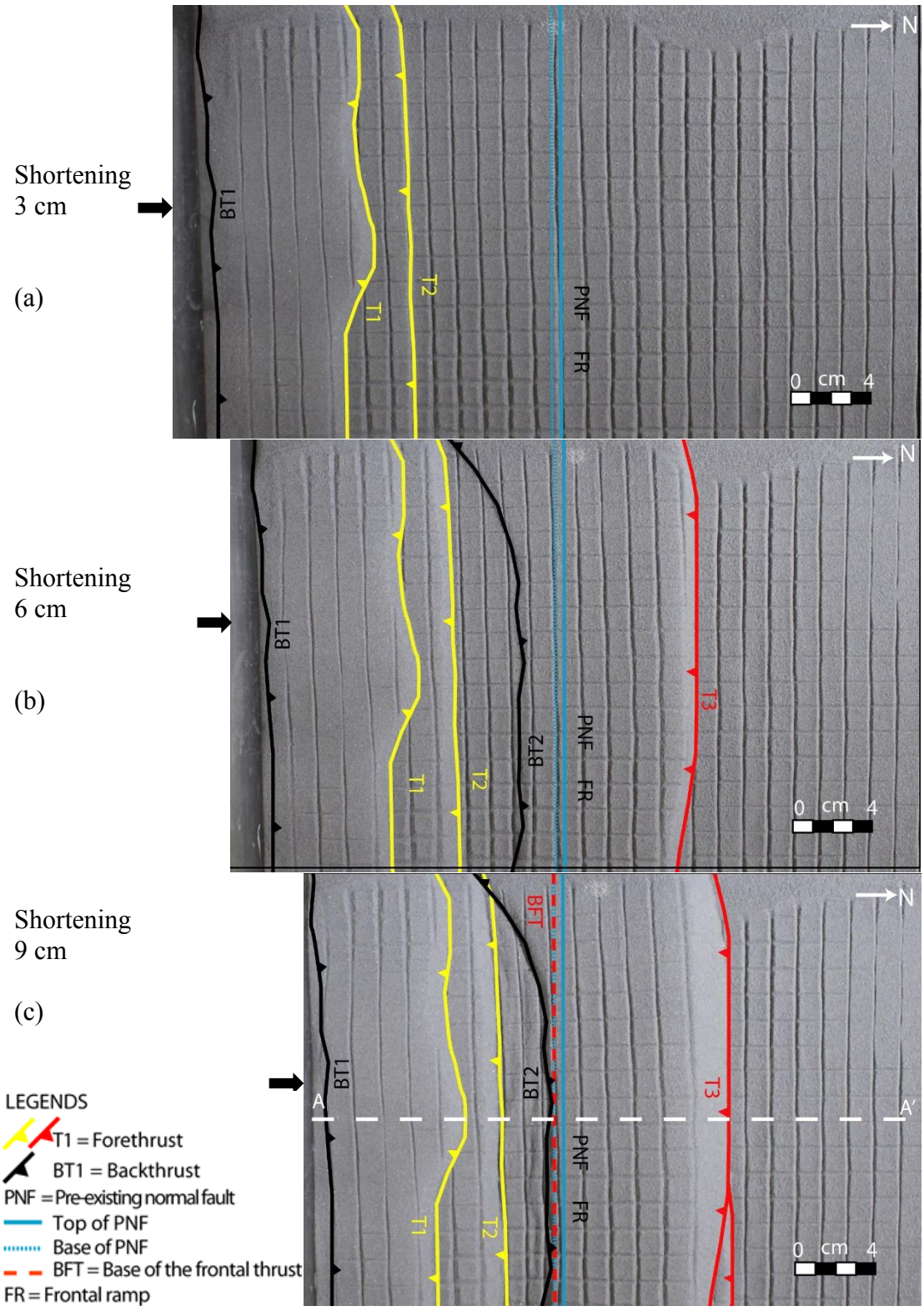

Figure 3.4 Progressive top photos of the ductile detachment on a frontal ramp experiment, model DDFR, with fault interpretation. (a) 3 cm shortening; (b) 6 cm shortening; (c) 9 cm shortening. A-A' shows the cross-section line for Figure 3.5.

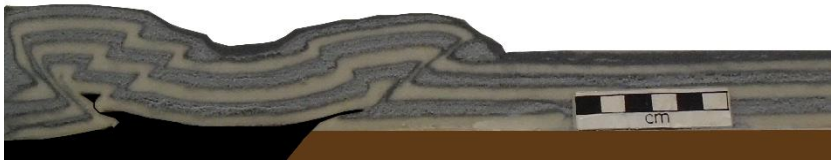

(a)

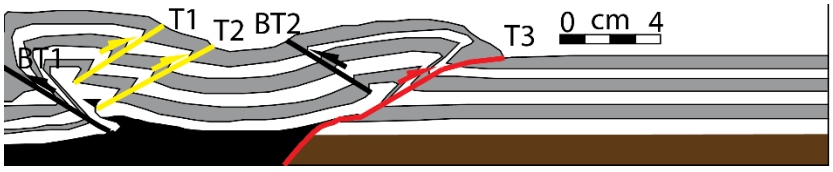

(b)

Figure 3.5 Cross-section A-A' of a ductile detachment on a frontal ramp experiment, model DDFR (see Figure 3.4 for location). T1-T3 = forethrusts, BT1-BT2 = backthrusts. (a) Section photo (b) line drawing of the section with fault interpretations.

3.3 Model BDOFR: Brittle detachment on a frontal ramp offset along a vertical transverse fault

Deformation was initially similar to the model BDFR with the formation of forethrusts T1 and T2 (Figure 3.6b). Additional shortening created the frontal thrusts T3 which first nucleated on the west frontal ramp and then nucleated on the east frontal ramp. Both segments climbed the frontal ramps and were connected by a transfer zone or a relay ramp at the offset frontal ramp boundary (Figure 3.6c). Movement on the frontal thrust rotated imbricate thrusts T1 and T2 to greater dips and the fold profile in the wedge became more rounded (Figure 3.7). After the formation of the frontal thrust T3, the wedge height increased in the west frontal ramp. The deformation front propagated farther toward the foreland in the east frontal ramp compared to the west frontal ramp (Figure 3.6). A symmetric frontal wedge formed on the frontal ramp to the east and a broad asymmetric wedge developed on the frontal ramp to the west. The slope of the imbricate wedge varied from 9 degrees to the east and 16 degrees to the west. The offset frontal ramp increased the taper angle on the west side. The key differences from the model BDFR are: (1) the formation of the transfer zone (2) hinterland structures on the backlimb bounded by backthrusts (BT1, and BT2) (Figure 3.7) and (3) more backthrusts formed in this model BDOFR compared to the model BDFR.

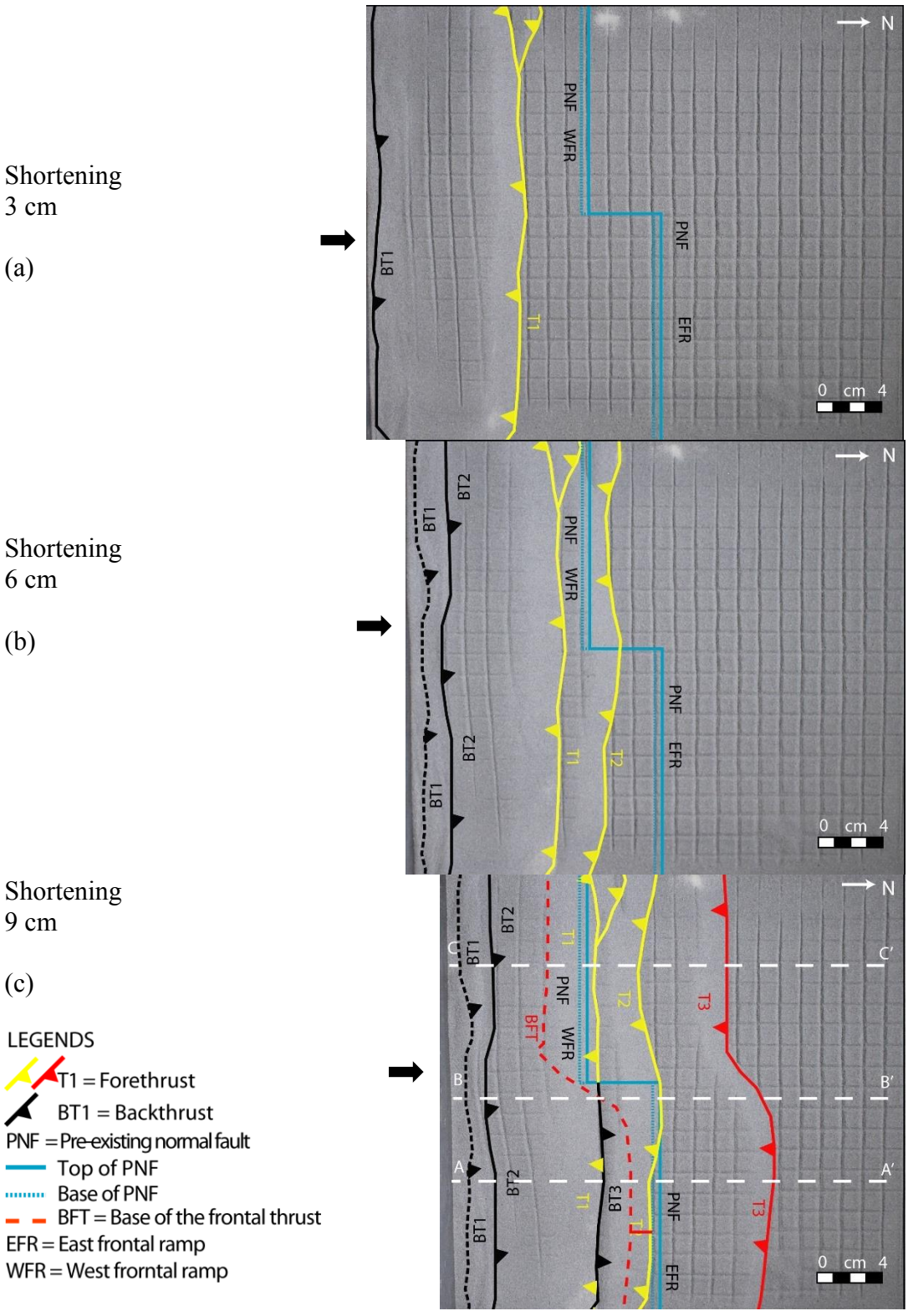

Figure 3.6 Progressive top photos of the brittle detachment on an offset frontal ramp, model BDOFR, with fault interpretation. (a) 3 cm shortening; (b) 6 cm shortening; (c) 9 cm shortening. A-A', B-B', and C-C' show the cross-sections lines for Figure 3.7.

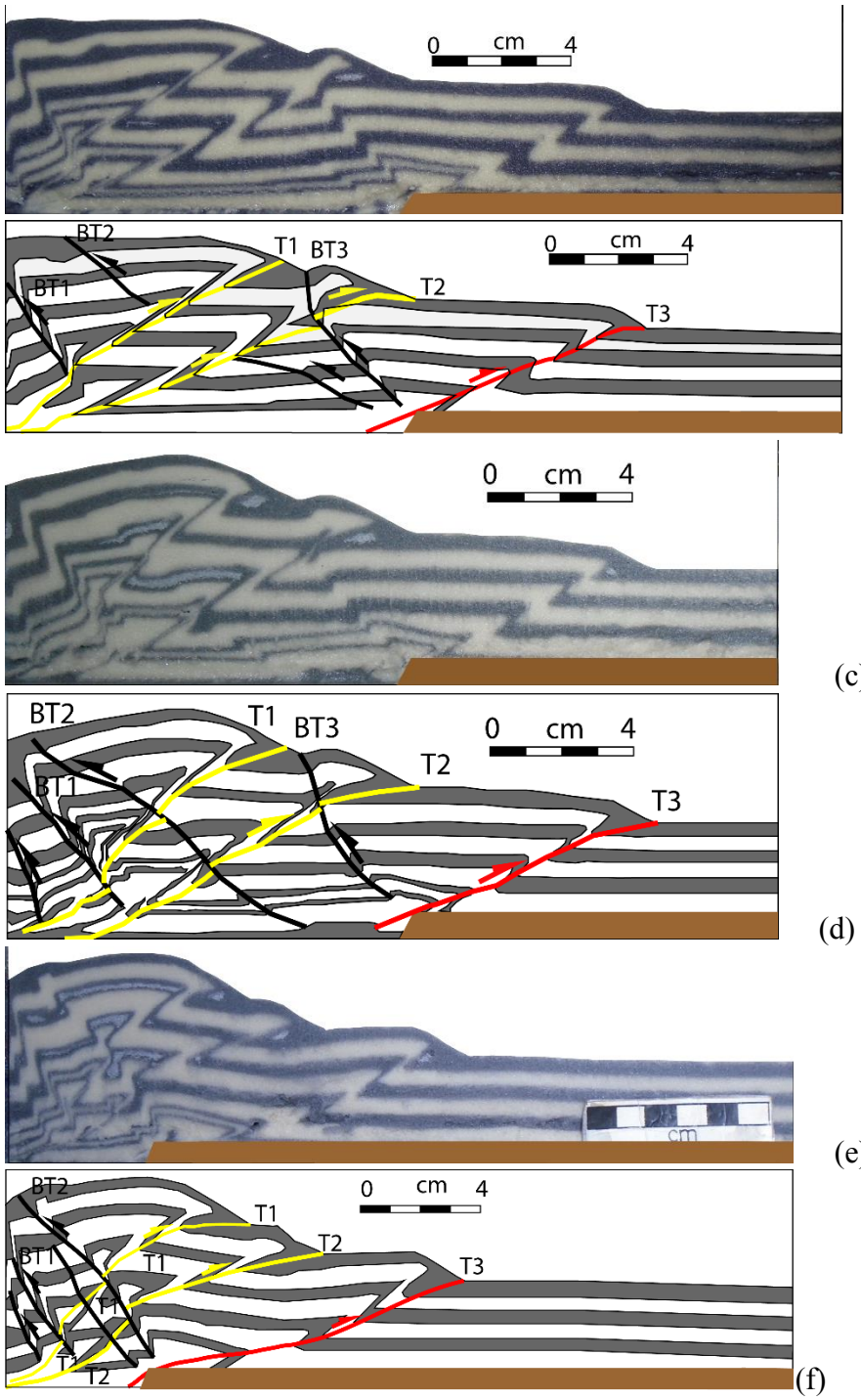

Figure 3.7 Cross-sections of the brittle detachment on offset frontal ramps, model BDOFR. (a) A-A' section; (b) line drawing of a; (c) B-B' section; (d) line drawing of c; (e) C-C' section; (f) line drawing of e (see Figure 3.6 for section locations).

3.4 Model DDOFR: Ductile detachment on a frontal ramp offset along a vertical transverse fault

The effect of the pre-existing offset frontal ramps on thrust geometry was seen from the very first forethrust T1 in the model DDOFR. This effect is obvious and earlier in the ductile detachment (model DDOFR) than its brittle detachment counterpart (model BDOFR) (Figure 3.8). As in the model BDOFR, the frontal thrust T2 first nucleated on the west frontal ramp and later connected to the frontal thrust formed on the east frontal ramp by a transfer zone (Figure 3.8). Frontal thrust T2 used the pre-existing normal fault ramps to form the frontal thrusts. The shape of the backthrust BT2 also followed the shape of the frontal thrust T2 (Figure 3.8). The backwedge height rose higher on the west frontal ramp after the formation of the frontal thrust T2. Backthrust BT2 had more displacement on the east frontal ramp area than on the west frontal ramp area. The transfer zone curvature on the model DDOFR was greater than that on the model BDOFR (Figure 3.8). The slope of the imbricate wedge increased from 7° in the east frontal ramp to 11° in the west frontal ramp.

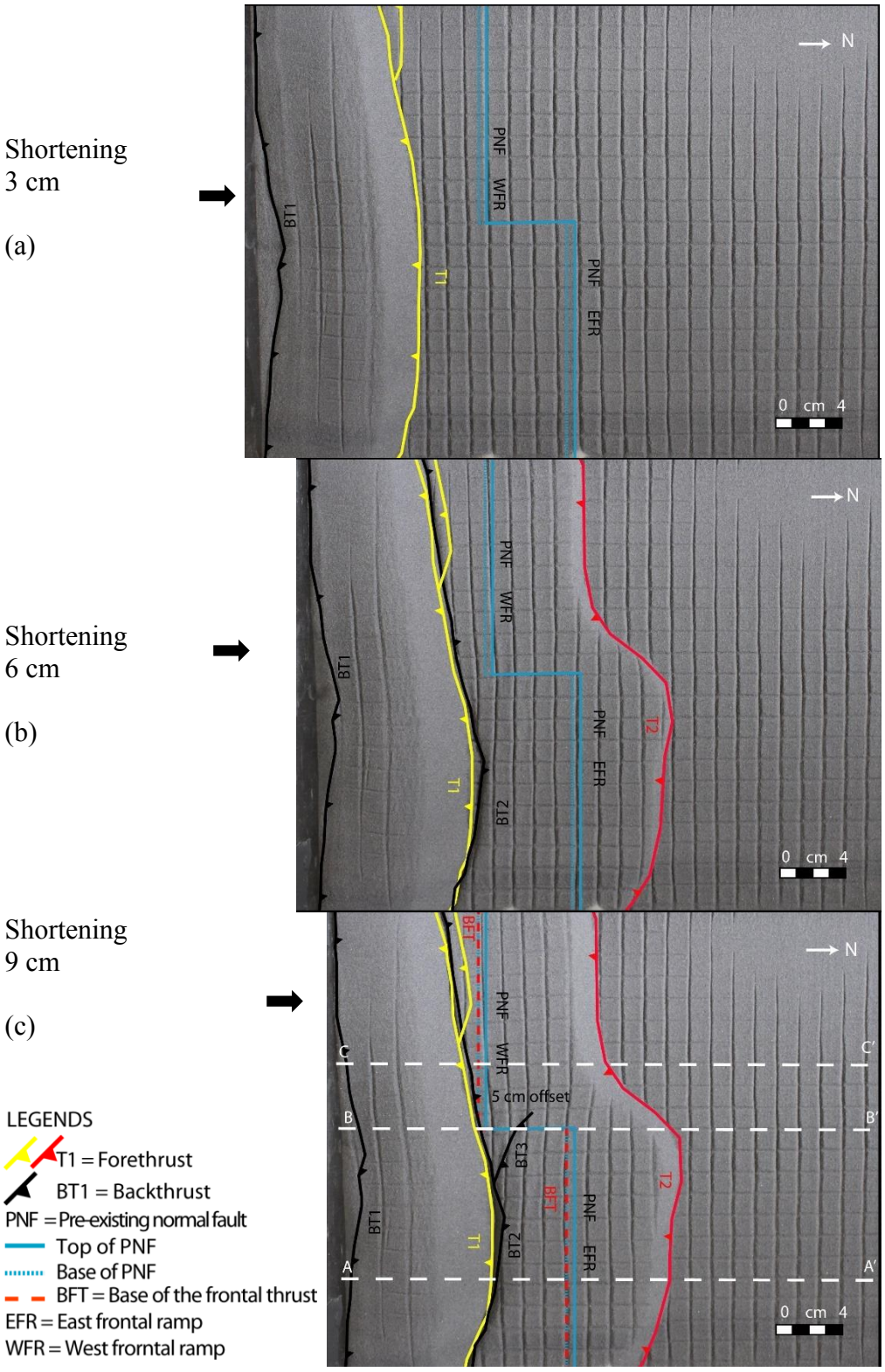

Figure 3.8 Progressive top photos of the ductile detachment on offset frontal ramps experiment, model DDOFR. (a) 3 cm shortening; (b) 6 cm shortening; (c) 9 cm shortening. A-A', B-B', and C-C' show the cross-sections lines for Figure 3.9.

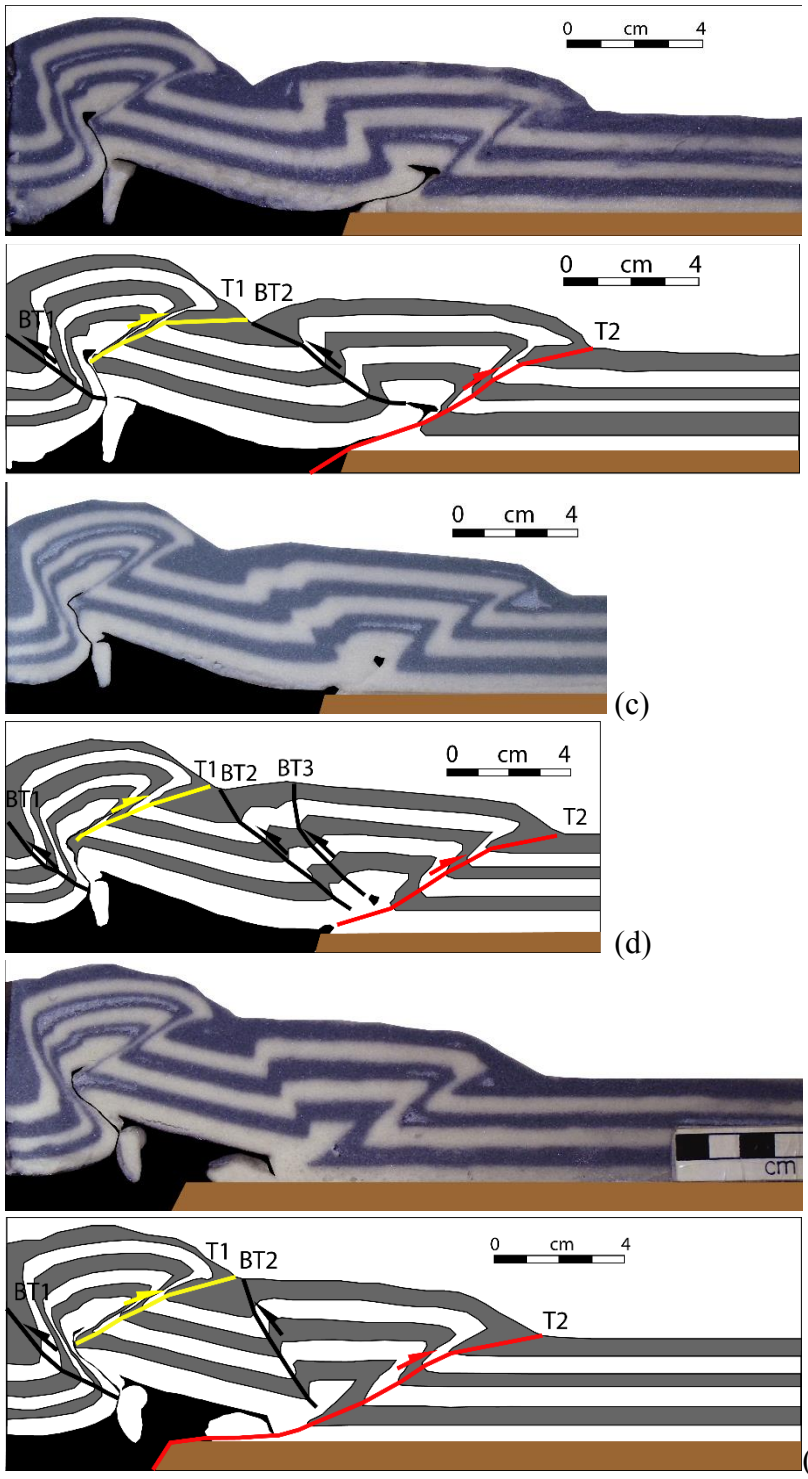

Figure 3.9 Cross-section of the ductile detachment on an offset frontal ramps experiment, model DDOFR. (a) A-A' section; (b) line drawing of a; (c) B-B' section; (d) line drawing of c; (e) C-C' section; (f) line drawing of e; (see Figure 3.8 for sections locations).

3.5 Model BDOBR: Brittle detachment on an oblique ramp trending 76 degrees

In this model, the normal fault was oblique to the direction of maximum shortening, trending 76 degrees. Formation of the first forethrust T1 was followed by T2 which branched from T1 and was in a more forward position to the east. Similarly, thrust T3 was followed by T4 which had a more forward position (Figure 3.10). The geometry of both T2 and T4 was in conformity with the oblique trend of the normal fault. Finally, the frontal thrust T5 showed a clear oblique trend, with the eastern part in a more forward position, and offset from the western part along an oblique transfer zone. The base of the frontal thrust was oblique and approximately parallel to the trend of the normal fault (Figure 3.11). The frontal thrust propagated 8.6 cm in the east and 10 cm in the west from the top of the normal fault.

Therefore, unlike previous models, the oblique trend of the normal fault was reflected not only in the final formed thrust, but also in the branching segments of earlier formed faults. The general trend of lateral propagation of the faults was from west to east. The taper angle in the east was 14°, and in the west, was 16°, so that the structural relief was greater to the west.

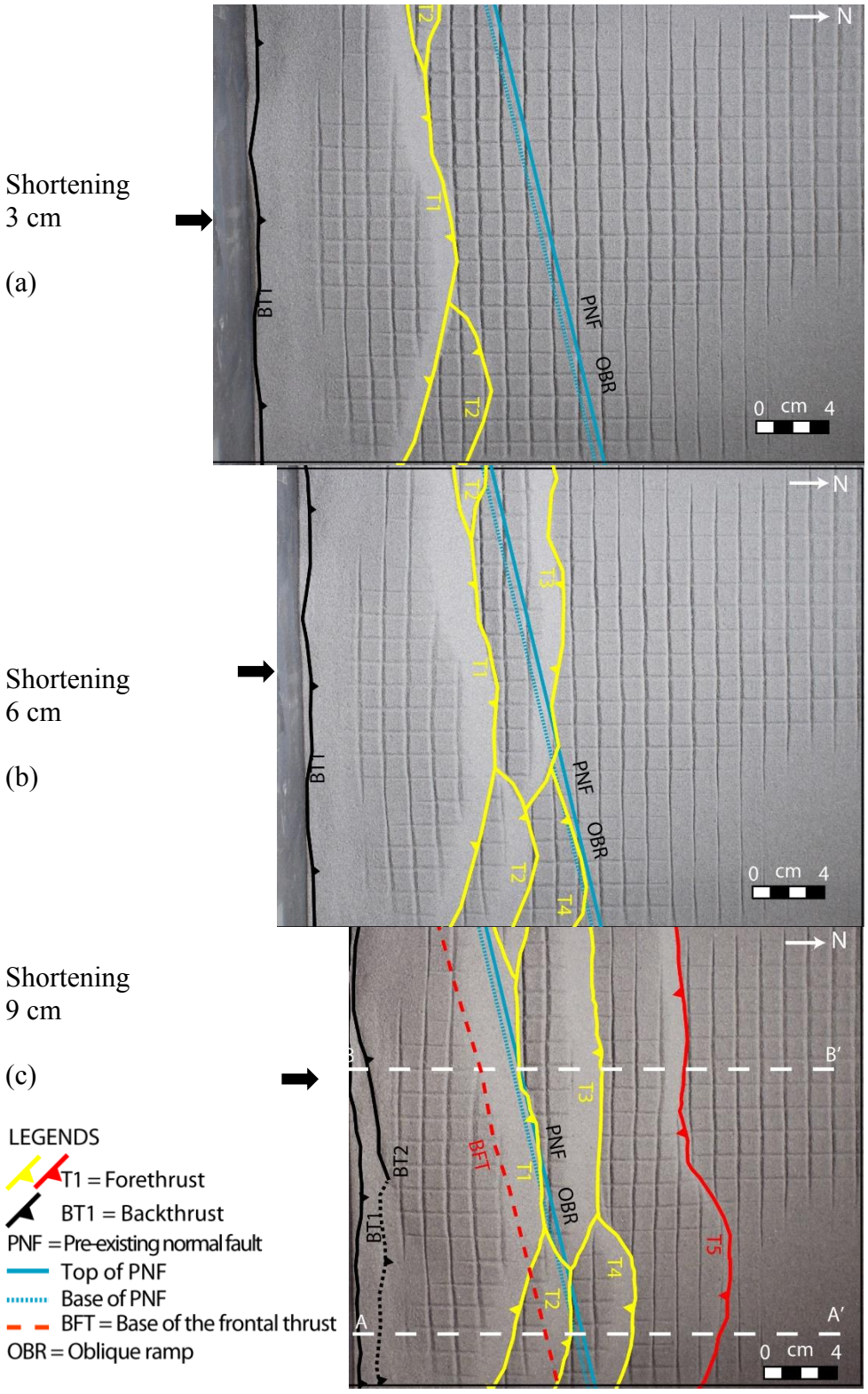

Figure 3.10 Progressive top photos of the brittle detachment on an oblique ramp trending 76 degrees experiment, model BDOBR with fault interpretation. (a) 3 cm shortening; (b) 6 cm shortening; (c) 9 cm shortening. A-A' and B-B' show the cross-sections lines for Figure 3.11.

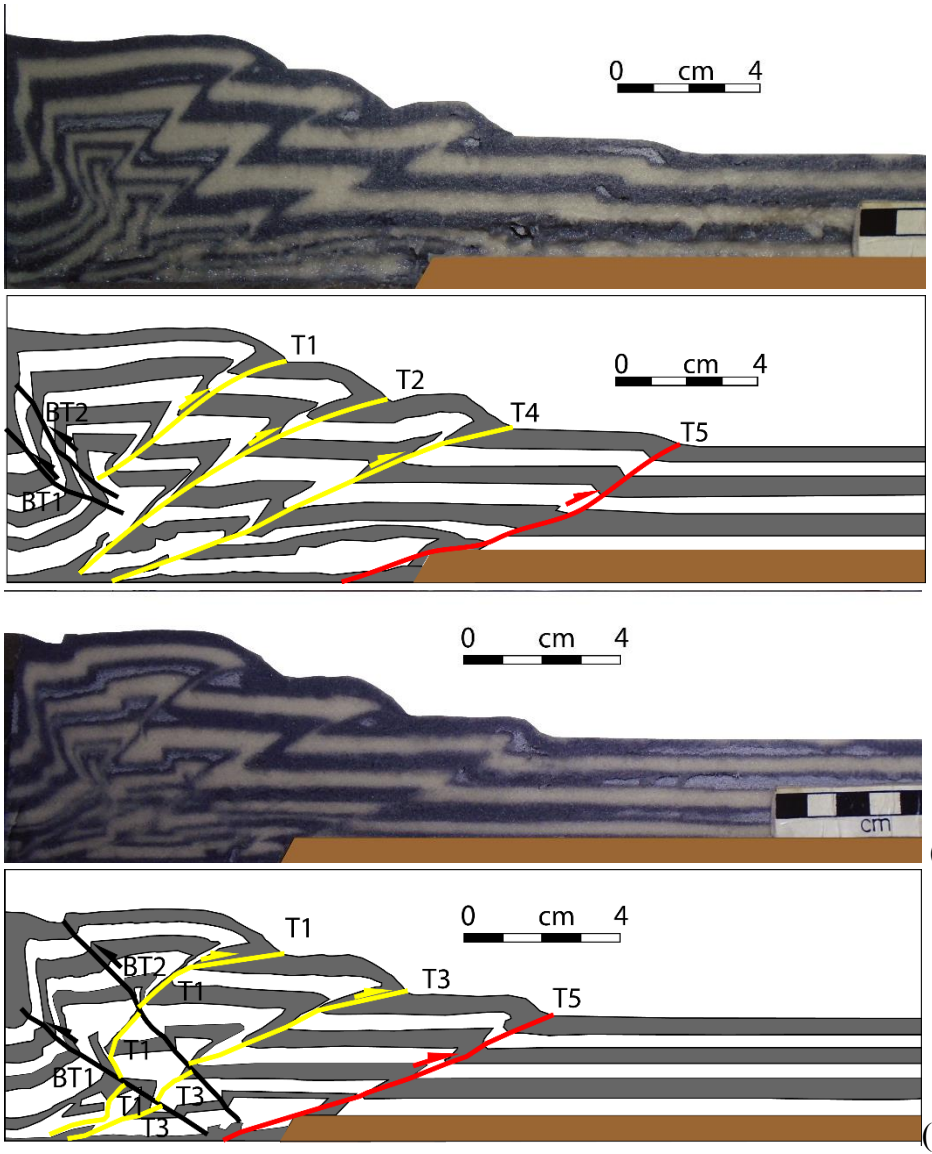

Figure 3.11 Cross-section interpretation of the brittle detachment on an oblique ramp trending 76 degrees experiment, model BDOBR (a) A-A' section; (b) line drawing of a; (c) B-B' section; (d) line drawing of c (see Figure 3.10 for sections locations).

3.6 Model DDOBR: Ductile detachment on an oblique ramp trending 76 degrees

The ductile detachment resulted in two faulted detachment folds verging towards the foreland, with related backthrusts. The trend of the first thrust T1 was normal to the direction of maximum shortening, and largely unaffected by the normal fault. The second thrust T2, however, had an oblique trend, similar to that of the normal fault (Figure 3.12). As in other ductile detachment models, the base of the frontal thrust was very close to the base of the normal fault, and almost parallel to it (Figure 3.13). Both forethrusts had curved geometries, and this is interpreted to be largely due to edge effects along the boundary of the model (Figure 3.12).

The structure developed a steeper wedge and greater relief to the west compared to the east. The development of the second thrust and the movement of the thrust sheet over the normal fault also occurred with a smaller amount of shortening (3 cm), compared to the brittle detachment experiment. This is due to the faster rate of propagation and lower taper angle of ductile detachment fold-thrust belts than those with a brittle detachment.

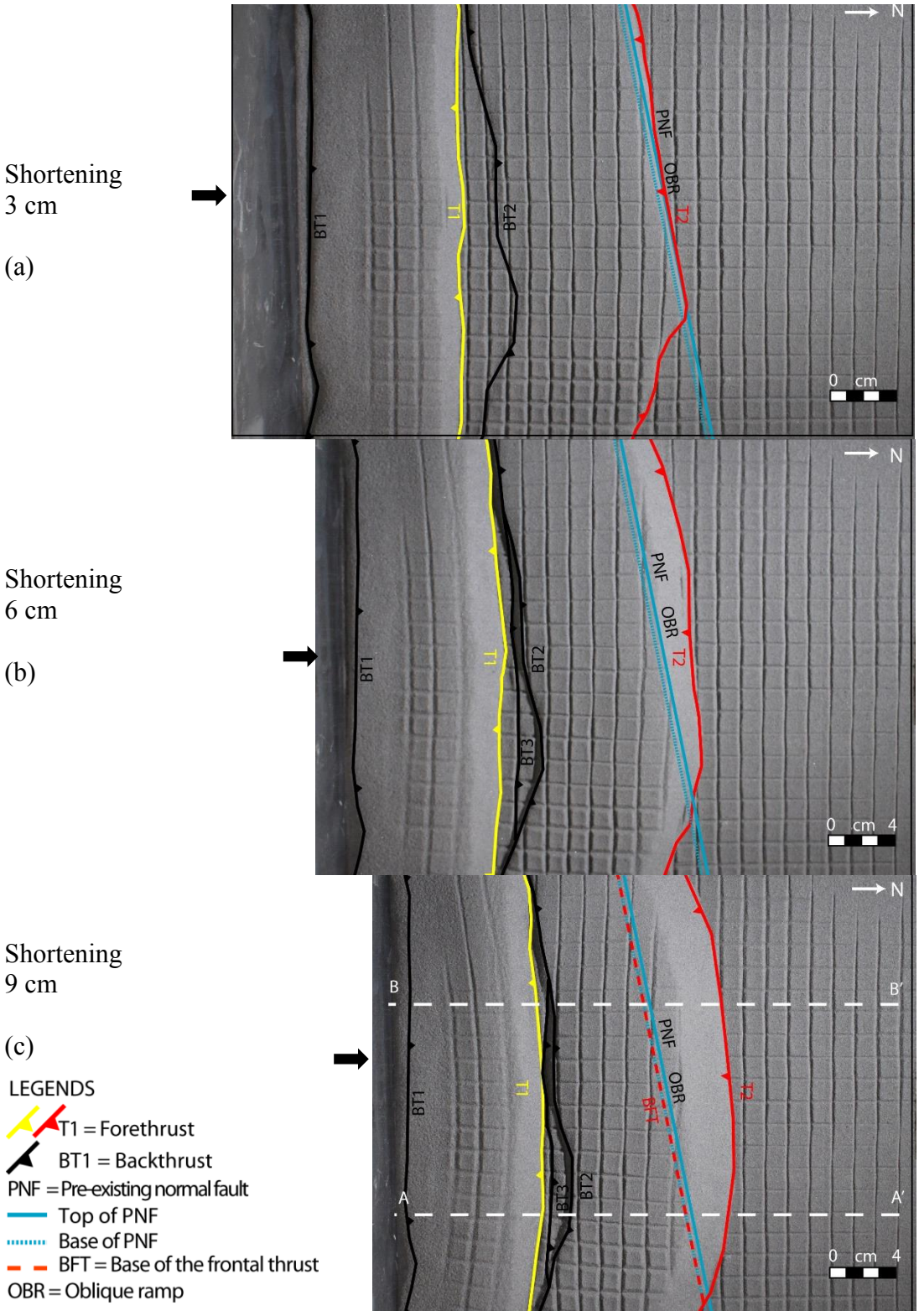

Figure 3.12 Progressive top photos of the ductile detachment on an oblique ramp trending 76 degrees experiment, model DDOBR with fault interpretation. (a) 3 cm shortening; (b) 6 cm shortening; (c) 9 cm shortening. A-A' and B-B' show the cross-sections lines for Figure 3.13.

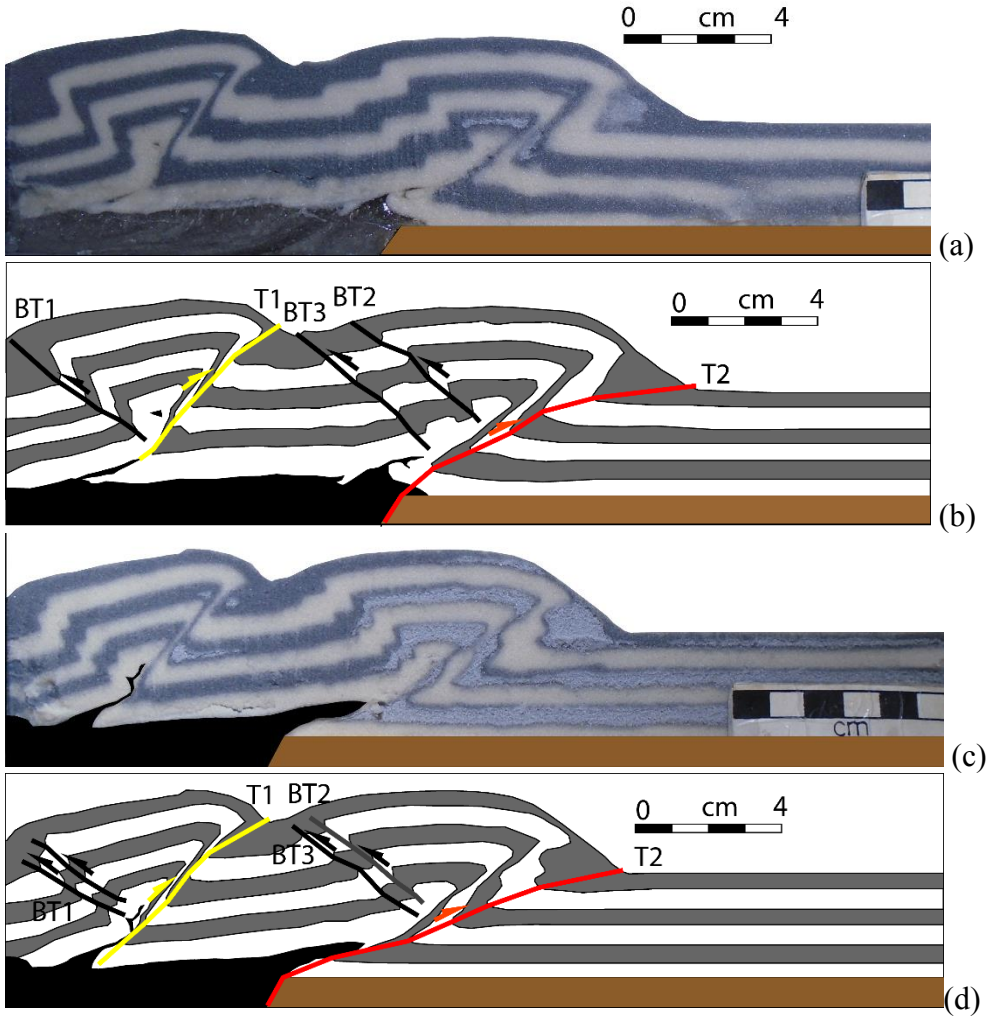

Figure 3.13 Cross-section interpretation of the ductile detachment on an oblique ramp trending 76 degrees experiment, model DDOBR. (a) A-A' section; (b) line drawing of a; (c) B-B' section; (d) line drawing of c (see Figure 3.12 for sections locations).

3.7 Model BDLR: Brittle detachment on a frontal ramp bounded by a vertical lateral ramp

In this model, a frontal ramp of the normal fault was bounded by a lateral ramp offset along a transverse fault (Figure 3.14). Here the deformation was initially similar to the model BDFR with the formation of forethrust T1. Additional shortening created the frontal thrusts T2 which first nucleated on the west frontal ramp and then it connected to the forethrust T1 on the east. Then the frontal thrust, T5, developed on the west frontal ramp and climbed the normal fault (Figure 3.14). The forethrusts T2 and T3, and forethrusts T5 and T4 were formed nearly at the equal position on the east and west in contrast to the more forward position of the forethrsuts in the model BDOBR. Thus, it confirms these forethrusts T4 and T5 were using the pre-existing normal faults' ramps as the thrust ramps. The frontal thrust, T6 was formed in the transverse fault area and was connected to the frontal thrusts T4 and T5 on the sides. However, this frontal thrust T6 did not use the transverse fault as a thrust ramp which as opposed to the model DDLR (Figure 3.15). Fault spacing between younger faults is smaller than the fault spacing between the older faults. Forward propagation of the forethrusts were hindered by the lateral ramps once the frontal thrusts climbed the frontal ramp because of the close spacing of the lateral ramps and the transverse fault. Though this effect was not observed in the ductile detachment, model DDLR which was because of the ductile detachment.

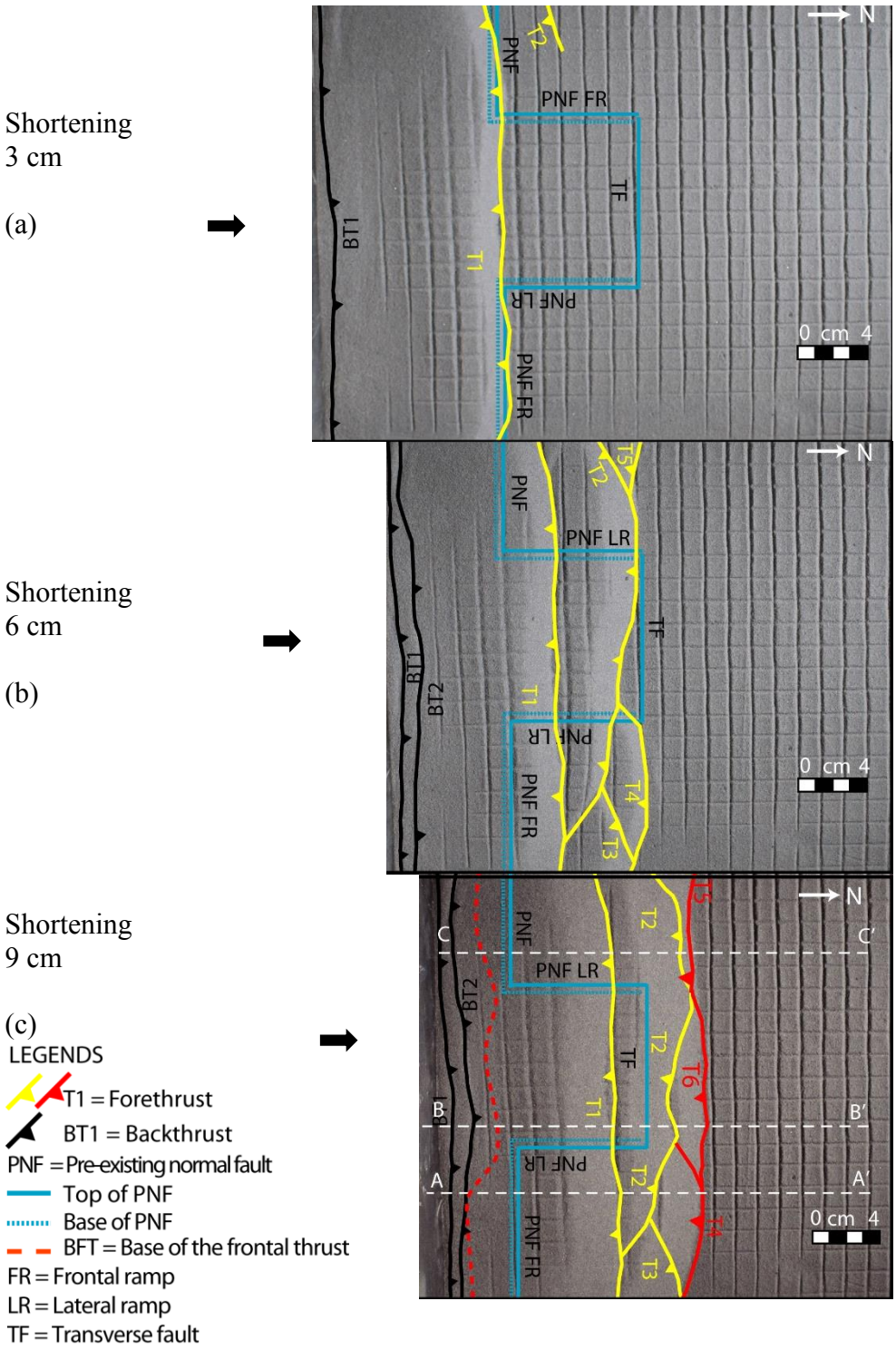

Figure 3.14 Progressive top photos of the brittle detachment on a frontal ramp bounded by a vertical lateral ramp, model BDLR. (a) 3 cm shortening; (b) 6 cm shortening; (c) 9 cm shortening. A-A', B-B' and C-C' show the cross-sections lines for Figure 3.15.

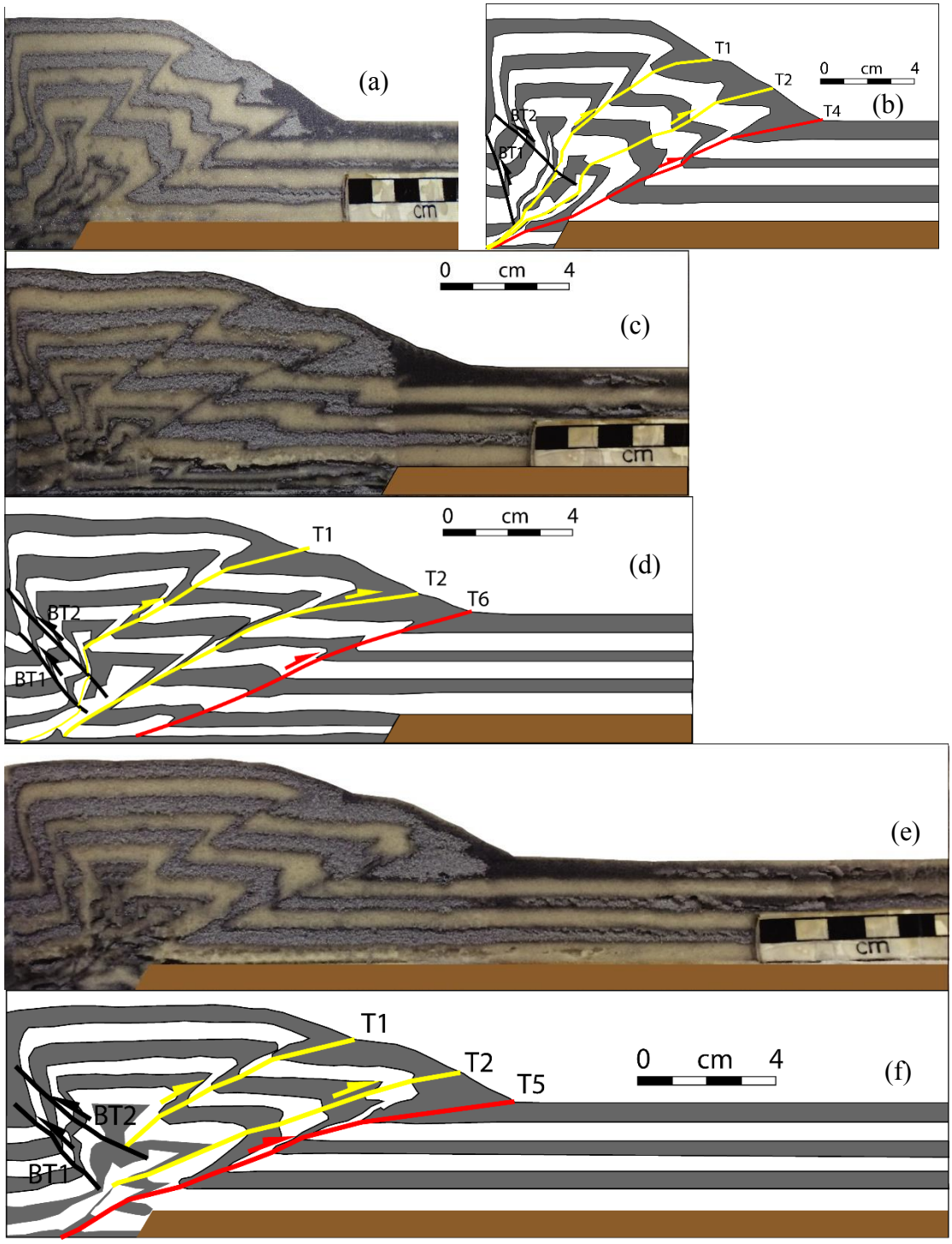

Figure 3.15 Cross-section interpretation of a brittle detachment on a frontal ramp bounded by a vertical lateral ramp, model BDLR. (a) A-A' section; (b) line drawing of a; (c) B-B' section; (d) line drawing of c; (e) C-C' section; (f) line drawing of e (see Figure 3.14 for sections locations).

3.8 Model DDLR: Ductile detachment on a frontal ramp bounded by a vertical lateral ramp

Deformation resulted in the formation of the foreland verging imbricate thrusts, T1 and T2 (Figure 3.16). Forethrust T3 nucleated on the west frontal normal ramp first and propagated laterally to the east. The frontal thrust T4 climbed the east frontal normal ramp and propagated westward. Later both T3 and T4 propagated almost equally to the foreland.

The geometry of frontal thrust T5 was influenced by that of the normal fault. T5 formed close to T3 and T4 along the eastern and western areas, but in a more frontal position in the central part of the model. This central segment connected with the eastern and western segments along oblique faults to form a curvilinear trace convex towards the foreland. The geometry of the fault followed the geometry of the normal fault and transverse normal fault ramps. The curvature of T5 and its structural relief increased with increasing shortening. The frontal wedge sloped at 24-29° along the lateral ramps and 23° on the frontal segment (Figure 3.17). The easier and farther thrust propagation is seen in the ductile detachment model DDLR than its counterpart model BDLR which was due to the ductile detachment.

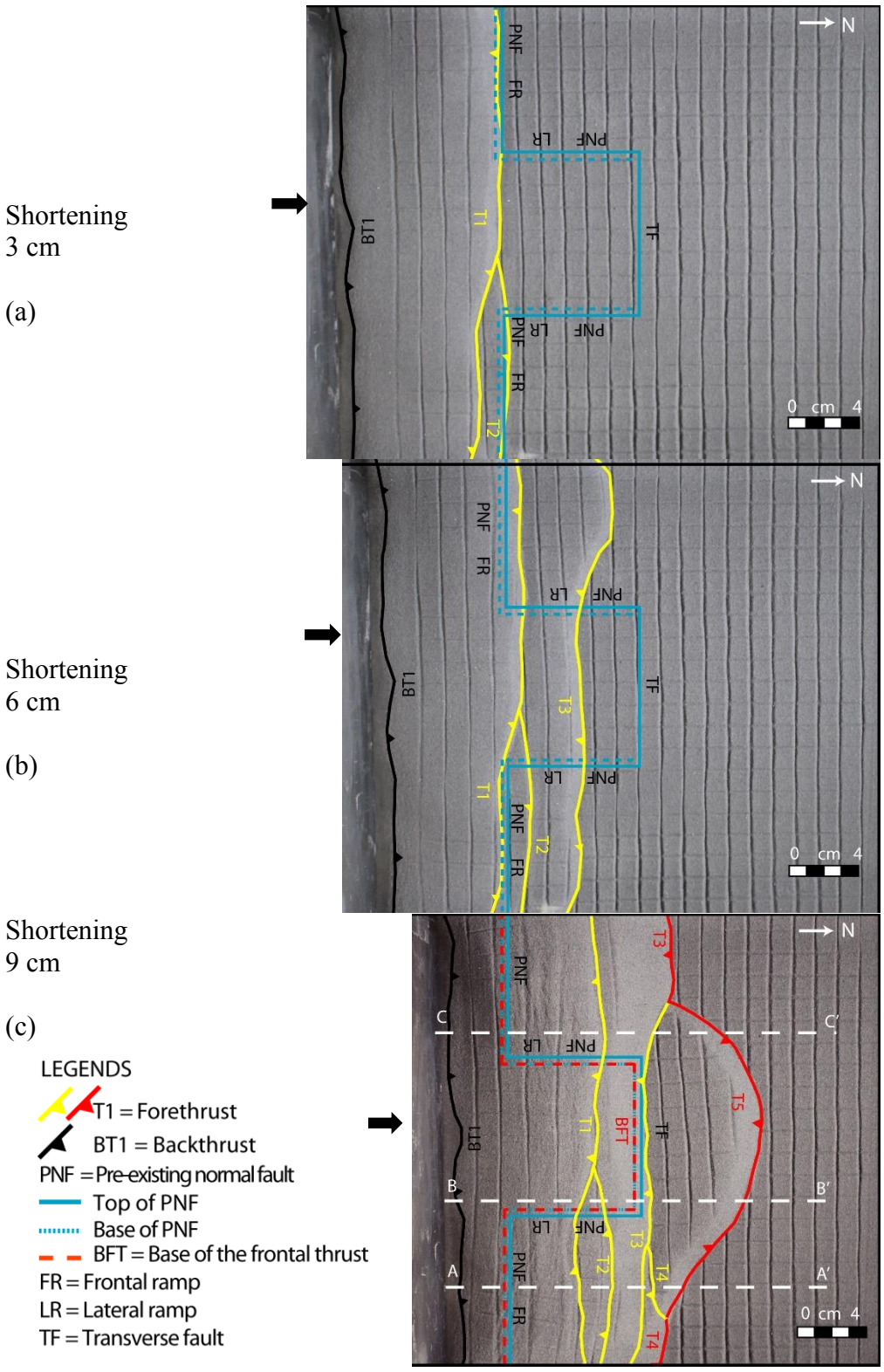

Figure 3.16 Progressive top photos of the ductile detachment on a frontal ramp bounded by a vertical lateral ramp experiment, model DDLR with fault interpretation. (a) 3 cm shortening; (b) 6 cm shortening; (c) 9 cm shortening. A-A', B-B', and C-C' show the cross-sections lines for Figure 3.17.

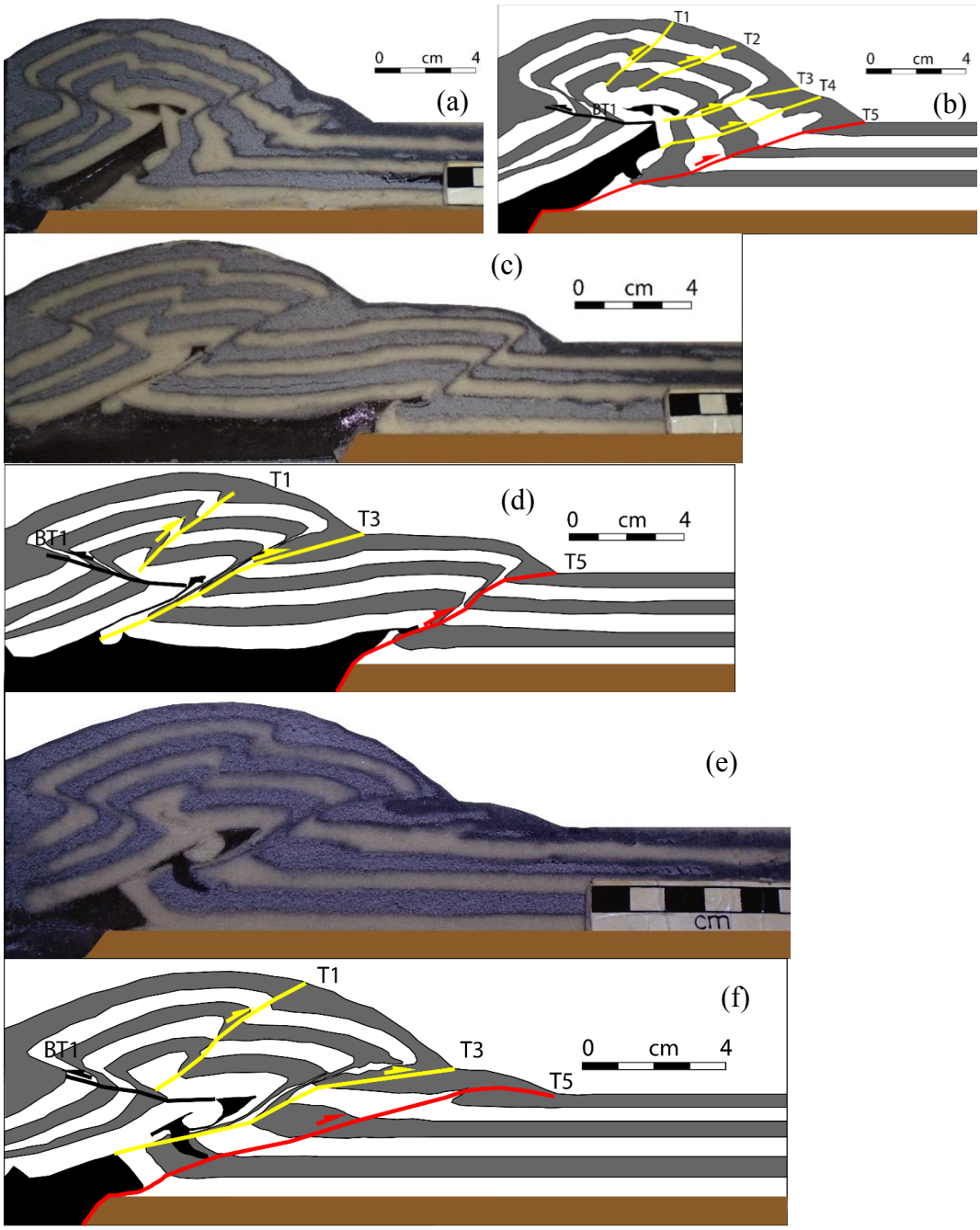

Figure 3.17 Cross-section interpretation of the ductile detachment on a frontal ramp bounded by a vertical lateral ramp experiment, model DDLR. (a) A-A' section; (b) line drawing of a; (c) B-B' section; (d) line drawing of c; (e) C-C' section; (f) line drawing of e (see Figure 3.16 for sections locations).

3.9 Model BDOBIR and BDCR: Brittle detachment on oblique intersecting ramps and brittle detachment on a curved ramp

Model BDOBIR used two oblique faults trending 76 degrees and making nearly 150 degrees at a intersection point (Figure 3.18). This system may result from an orthorhomic strain pattern [*Reches*, 1978]. BDCR used a gently curved normal fault ramp, which may result from two oblique faults connecting along a smooth curve. In both cases, duplex structures with stacked faults were formed (Figure 3.18 & Figure 3.20). The trends of early formed thrust faults were unaffected by the geometry of the normal faults, and developed a stacked thrust faults on duplex structures (Figure 3.19 & Figure 3.21). The frontal thrust ramped up approximately 7.3 cm from the top of the normal fault for the intersecting normal faults, and 7.6 cm from the top of the normal fault for the curved fault.This fault showed a very similar geometry trend to the normal fault with an angular geometry in the first model and a more curved geometry in the second (Figure 3.19 & Figure 3.21).

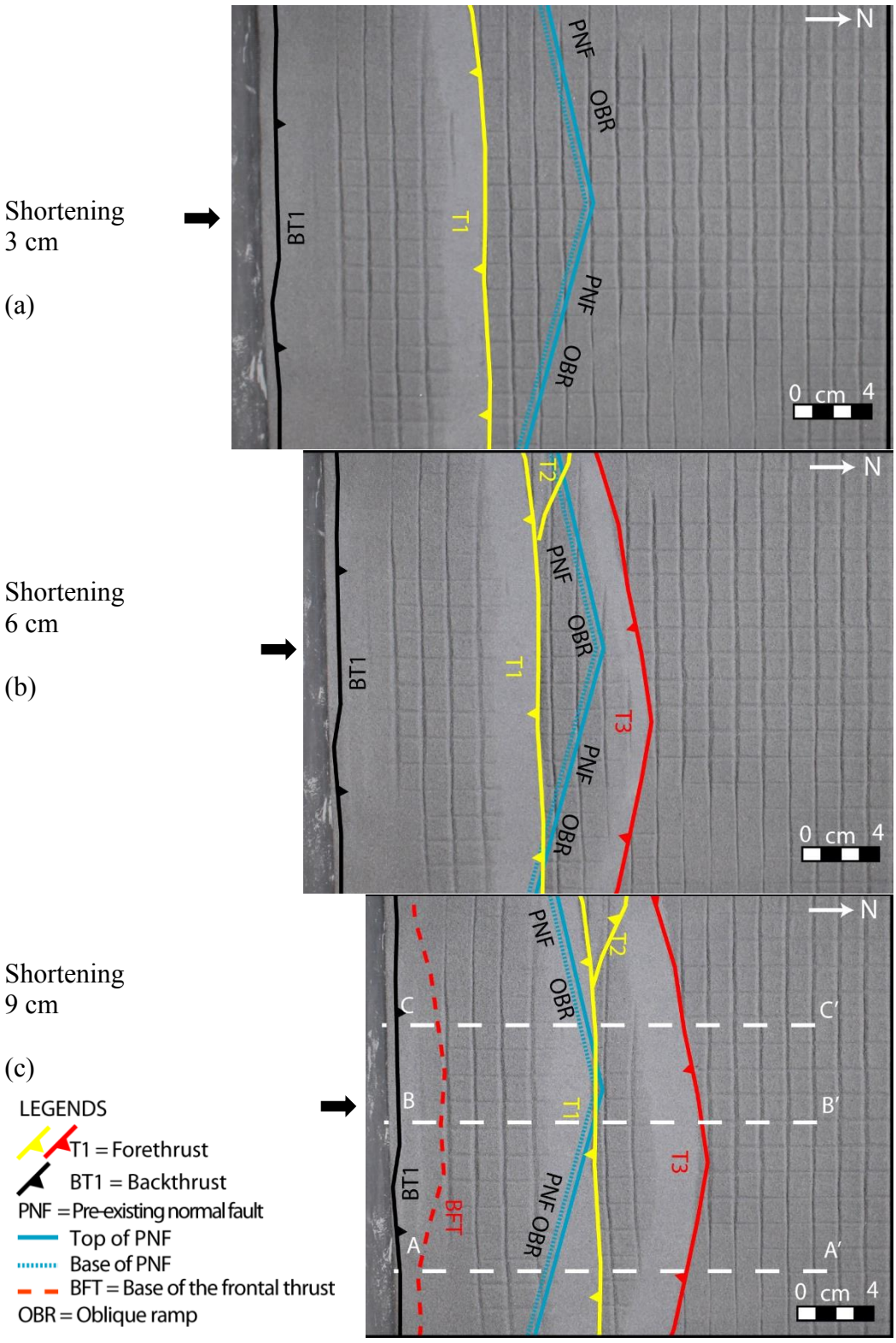

Figure 3.18 Progressive top photos of the oblique intersecting ramps on a brittle detachment experiment, model BDOBIR with fault interpretation. (a) 3 cm shortening; (b) 6 cm shortening; (c) 9 cm shortening. A-A', B-B', and C-C' show the cross-sections lines for Figure 3.19.

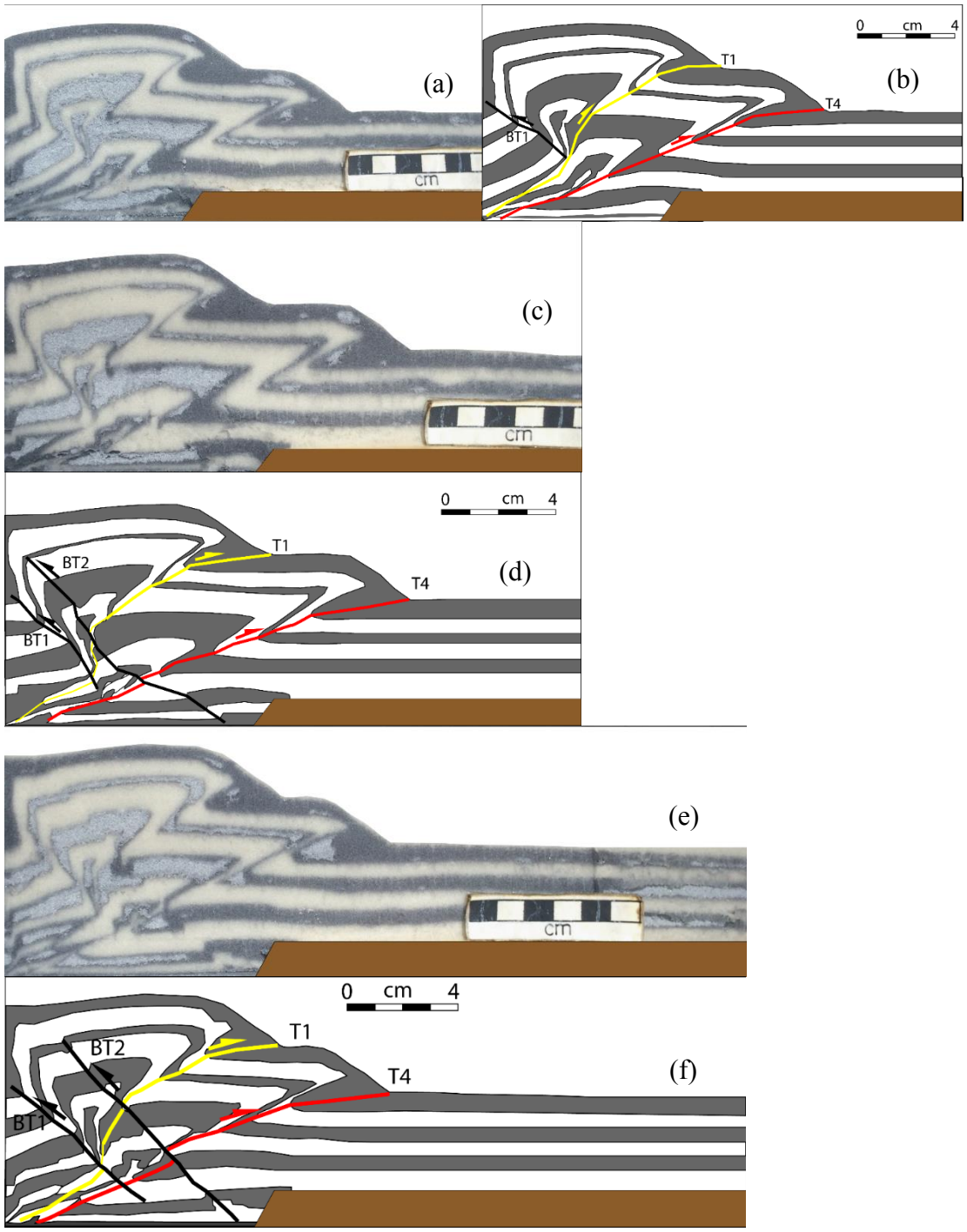

Figure 3.19 Cross-section interpretation of brittle detachment on oblique intersecting ramps experiment, model BDOBIR. (a) A-A' section; (b) line drawing of a; (c) B-B' section; (d) line drawing of c; (e) C-C' section; (f) line drawing of e (see Figure 3.18 for sections locations).

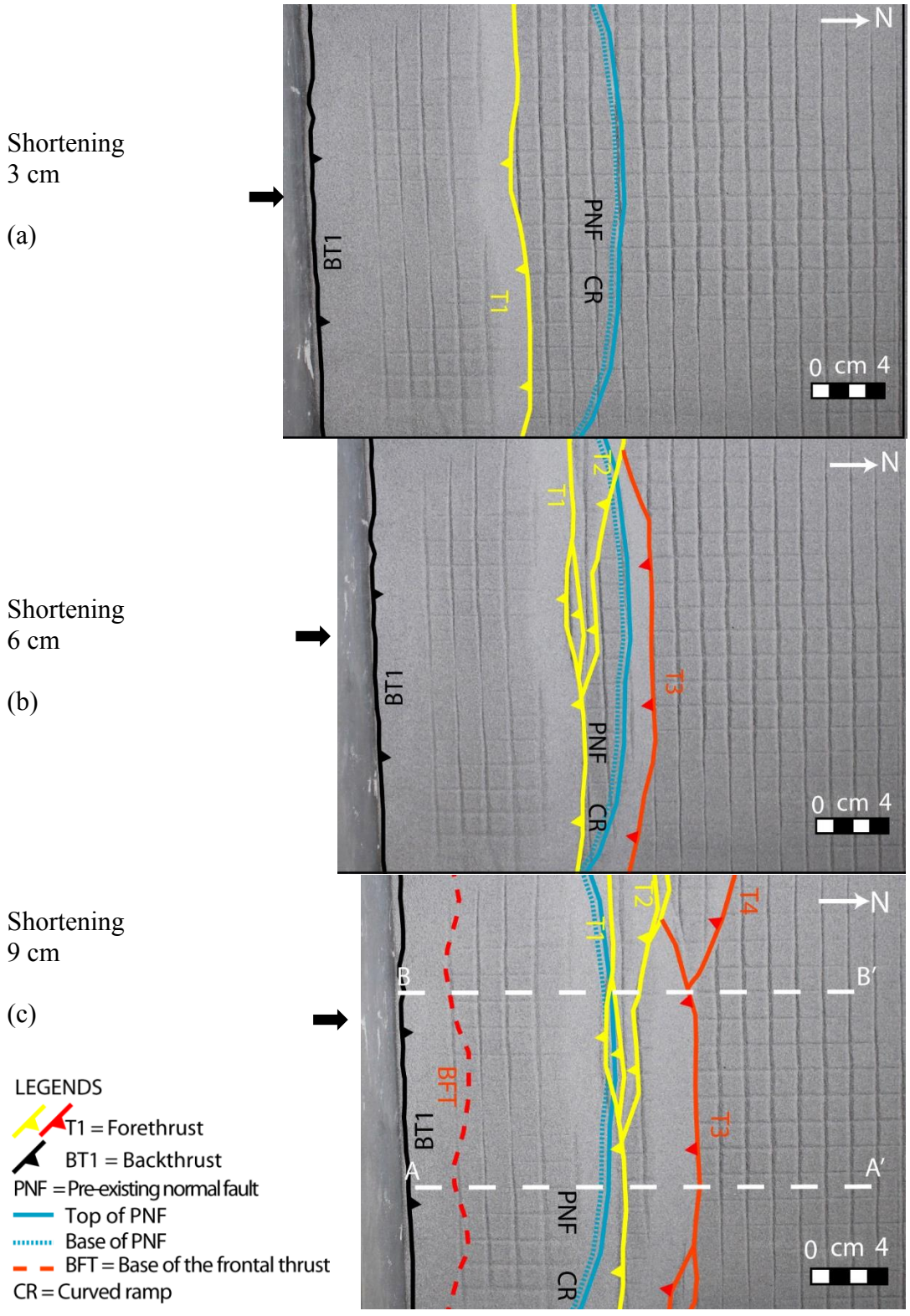

Figure 3.20 Progressive top photos of the brittle detachment on a curved ramp experiment, model BDCR with fault interpretation. (a) 3 cm shortening; (b) 6 cm shortening; (c) 9 cm shortening. A-A' and B-B' show the cross-sections lines for Figure 3.21.

(a)

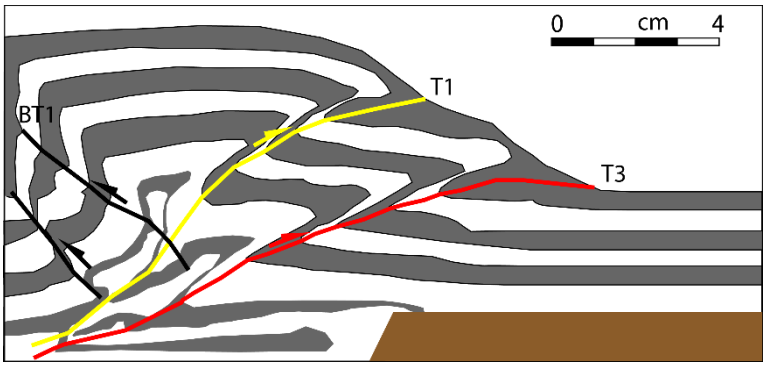

(b)

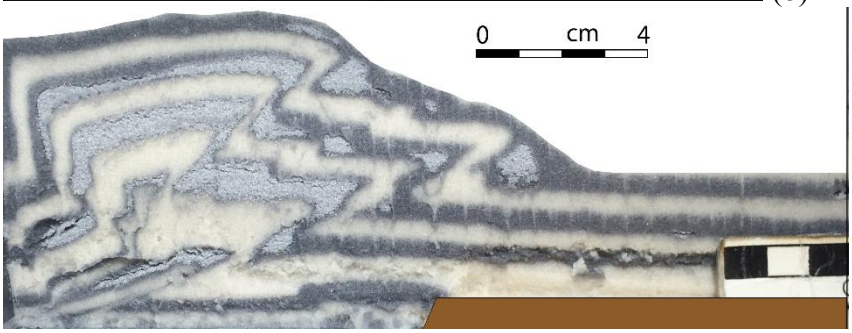

(c)

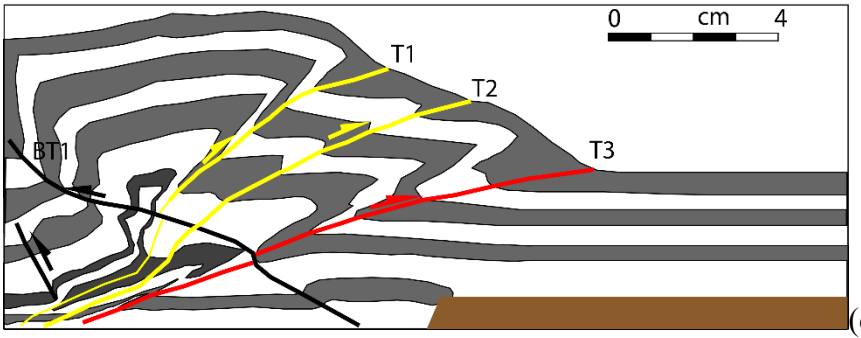

(d)

Figure 3.21 Cross-section interpretation of the curved ramp on a brittle detachment experiment, model BDCR. (a) A-A' section; (b) line drawing of a; (c) B-B' section; (d) line drawing of c (see Figure 3.20 for sections locations).

3.10 Model DDCR: Ductile detachment curved ramp

Model DDCR used a ductile detachment and a curved ramp, except there was greater curvature of the normal fault ramp than in model BDCR (Figure 3.22). Deformation resulted in two faulted detachment folds vergent towards the foreland with associated back thrusts. The first thrust had a linear trend, but thrust T2 developed a curved shape parallel to the trend of the curved normal fault. The frontal thrust T2 was formed when the model was shortened to 3 cm, so that it developed earlier than in the brittle detachment model. It propagated 10 cm from the top of the normal fault in the middle of the model. Progressive contraction translated the frontal wedge to the foreland and increased the height of the wedge. The backthrust BT2 (Figure 3.23) was formed south of the frontal thrust T2 and followed the shape of the frontal thrust T2.

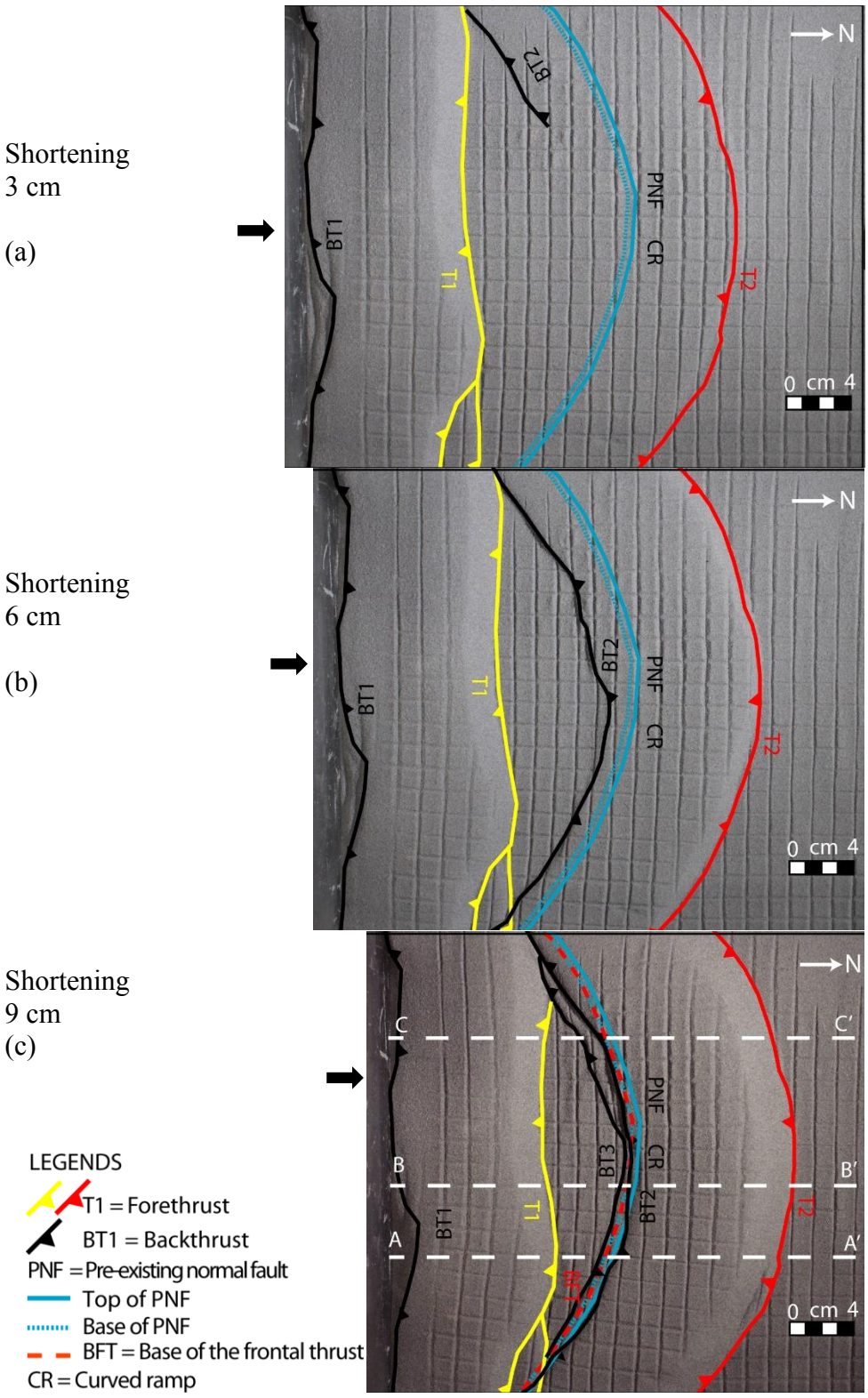

Figure 3.22 Progressive top photos of the ductile detachment on a curved ramp experiment, model DDCR with fault interpretation. (a) 3 cm shortening; (b) 6 cm shortening; (c) 9 cm shortening. A-A', B-B', and C-C' show the cross-sections lines for Figure 3.23.

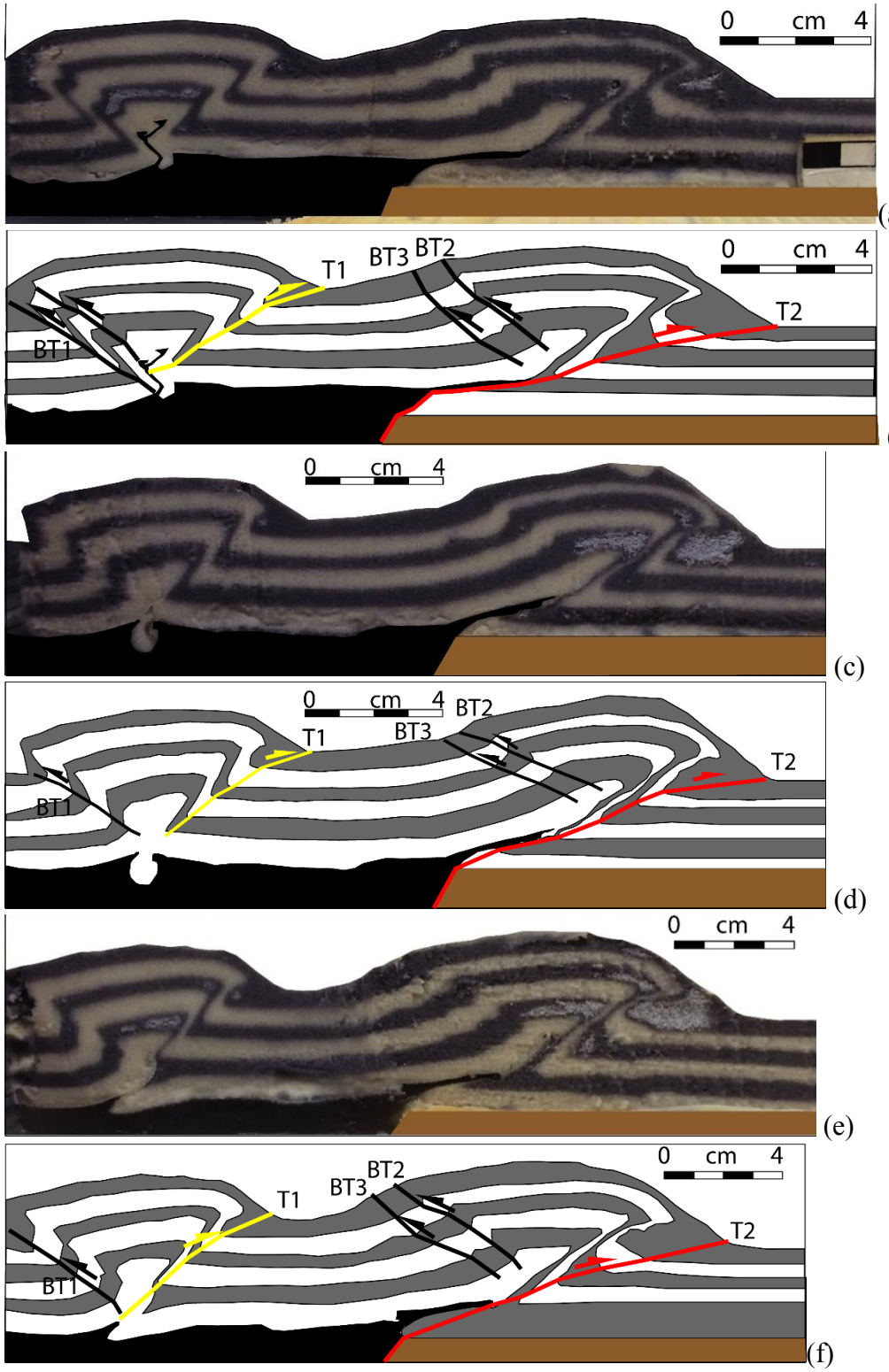

Figure 3.23 Cross-section interpretation of the ductile detachment on a curved ramp experiment, model DDCR. (a) A-A' section; (b) line drawing of a; (c) B-B' section; (d) line drawing of c; (e) C-C' section; (f) line drawing of e (see Figure 3.22 for sections locations).

4 Discussions- Natural Structures

4.1 Pine Mountain Thrust Sheet

4.1.1 Field structures

The Appalachians Mountains were formed by a series of orogenic events in the Paleozoic, of which the late Paleozoic Alleghenian orogeny is the dominated one affecting the foreland thrust belt in the southern Appalachians. The Pine Mountain thrust bounds the southern Appalachian thrust sheet to the northwest. The thrust sheet associated with the thrust fault was bounded by the Wallen Valley and Hunter Valley thrusts to the southeast (Figure 4.1). Two tear faults, the Russell Fork and Jacksboro faults bound the Pine Mountain thrust to the northeast and southwest, respectively (Figure 4.1). In a general section, the Pine Mountain thrust brings the Cambrian Rome Formation over the Devonian Chattanooga Shale and then to the surface. An anticline-syncline pair is formed as a result of the movement of the thrust sheet over the ramp.

Stratigraphic units in the Pine Mountain Thrust can be divided into a number of lithotectonic units which controls the geometry of the structures. It includes the Precambrian crystalline basement and Precambrian to Cambrian basal clastic sequence, which is generally not involved in the thin-skinned deformation. The Lower Cambrian Rome Formation and the Middle to Upper Cambrian Conasauga Formation consist mostly of incompetent shales and carbonates. The basal detachment of the thrust belt is located in the lower part of the Rome Formation. The Cambrian Maynardville Formation and the Cambro-Ordovician, the Knox Group, consist of interlayered

(a)

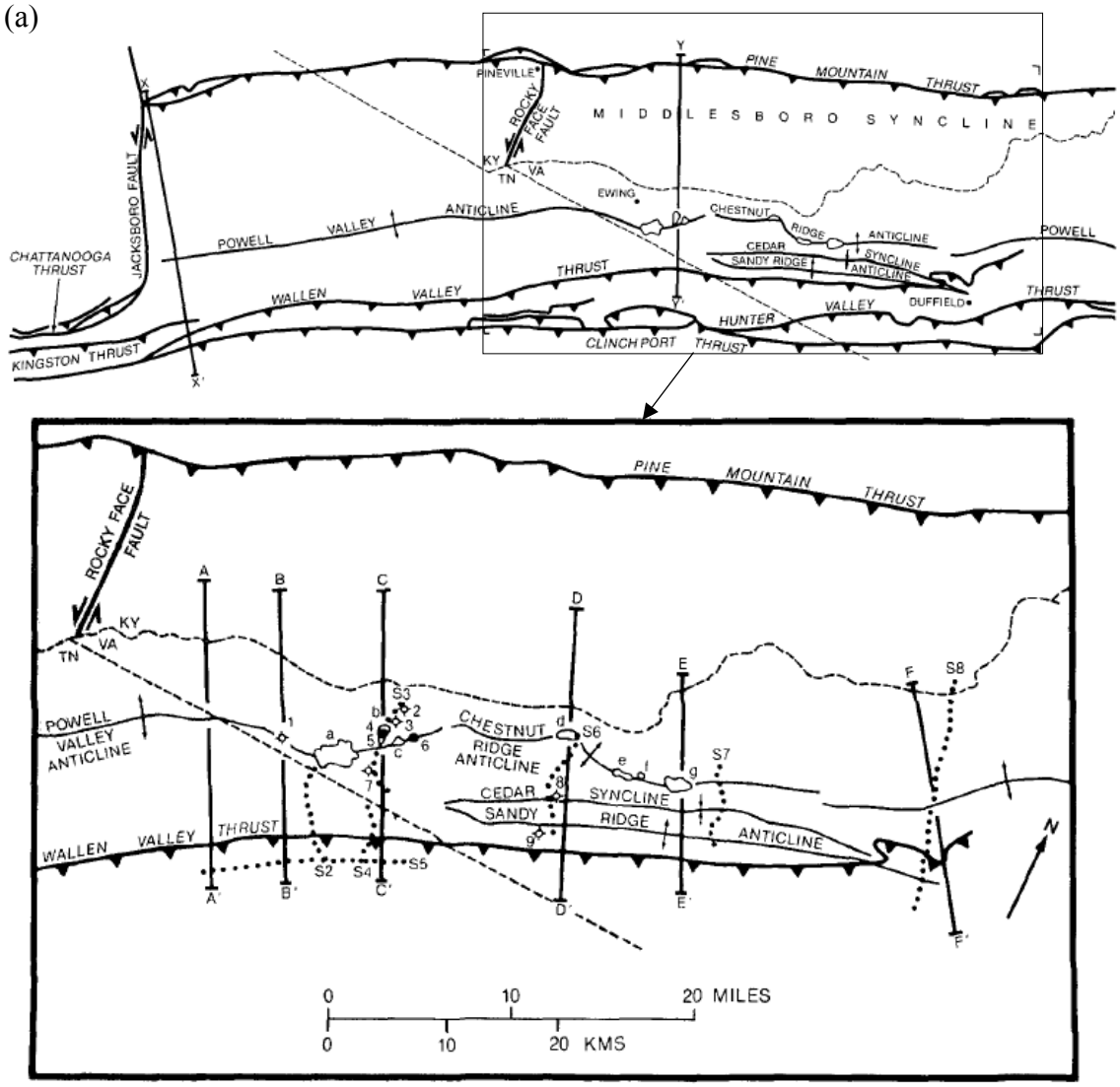

(b)

Figure 4.1 (a) Geological map of the Pine Mountain thrust sheet showing the major folds and thrusts. (b) Inset map: Structure map of the center fenster area of the Pine Mountain thrust sheet showing the location of a cross-section C-C' (Figure 4.2). S2 to S8 are seismic profiles. a = Chestnut Ridge fenster, b = Martin Creek fenster, c = Possum Hollow fenster, d = Bethel fenster, e = Big Fleenortowrn fenster, f = Sulphur Spring fenster, g = Town Branch fenster, 1 = Brooks well, 2 = Rosenbaum well, 3 = H.B. Nolan well, 4 = R. L. Bales well, 5 = Hobbs well, 6 = Hensley well, 7 = L. S. Bales well, 8 = McClure well, 9 = Snodgrass well [*Mitra*, 1988].

dolomites and limestones which are competent units that deform mainly by fracturing and imbrication. In the central area of the Pine Mountain thrust, the Maynardville Formation is separated from the Conasauga Formation by an intermediate detachment. The Middle Ordovician Chickamauga Group consists dominantly of limestones which deform by minor folding and imbrication as well as fracturing and pressure solution. The Upper Ordovician units consist of an inhomogeneous sequence of thin-bedded shales alternating with limestones and sandstones. The Devonian Chattanooga Formation consists of the upper detachment for the thrust belt. The Mississippian and Pennsylvanian units consist mostly of competent limestone and sandstone.

The Pine Mountain thrust is folded by underlying thrust forming horses and duplexes that result in erosional fensters in some places. The two major oil-producing areas include the Sulphur Springs and Big Fleenortown fensters in the Ben Hur area, and the Martin Creek, Chestnut Ridge and Possum Hollow fenster in the Rose Hill area. The structure consists of three overlapping ramp anticlines associated with three thrust sheets in the Martin Creek fenster area (Figure 4.2). The three thrusts sheets are the Pine Mountain, Bales I, and Bales II sheets. The Pine Mountain thrust climbs from the Cambrian Rome Formation to the base of the Cambrian Maynardville Limestone of the Conasauga Formation, and finally to the base of the Devonian Chattanooga Shale. The Bales I thrust climbs from the Rome Formation to the base of the Chattanooga Shale which folds the Pine Mountain thrust with steepening of the frontal limb with dip exceeding 60°.

Seismic data show that the location of the Bales II is related to a pre-existing basement normal fault (Figure 4.3). The thrust brings the Rome Formation over the Conasauga

Formation. Moreover, the folding associated with the Bales II thrust creates the irregularities in the geometry of the Bales I thrust. *Mitra* [1988] constructed and interpreted several cross-sections in the Pine Mountain thrust sheets by using well, seismic, and field data. These cross-sections are then plainspastically restored to check that they are balanced and to estimate the shortening in each section. They are also used to construct maps showing the geometry of the major thrusts in the deformed and restored sections (Figure 4.2). The cross section represented in Figure 4.2 incorporates surface data and seismic reflection profiles S3 and S4 (Figure 4.3) and confirms the presence of the pre-existing normal fault. *Mitra* [1986a] suggested the role of additional lateral and oblique thrust ramps and tear faults in the evolution of the Pine Mountain thrust geometry. Kinematic interpretation of the geometry of the Pine Mountain thrust changed northeastward from a single thrust ramp to a double ramp. The displacement of the ramp may have been caused by the minor discontinuity or buttressing effect from a pre-existing normal fault and a change in the regional dip of the Rome detachment.

4.1.2 Comparison to the experimental model

Martin Creek fenster area (Figure 4.2) resembles the brittle detachment on the frontal ramp experiment (Figure 3.1 & Figure 3.2) (model BDFR), as suggested by the parallel orientation of the Clinch Port, Wallen Valley, and Pine Mountain thrust sheets in the map view (Figure 3.1). Note the fault spacing also increases from the Clinch Port thrust to the Pine Mountain thrust which is also observed in the model BDFR. The frontal thrust, Bales II thrust has a small amount of slip, because it is in its early stage of deformation, so the model BDFR does not exactly replicate this thrust, in which the frontal thrust had undergone significant shortening.

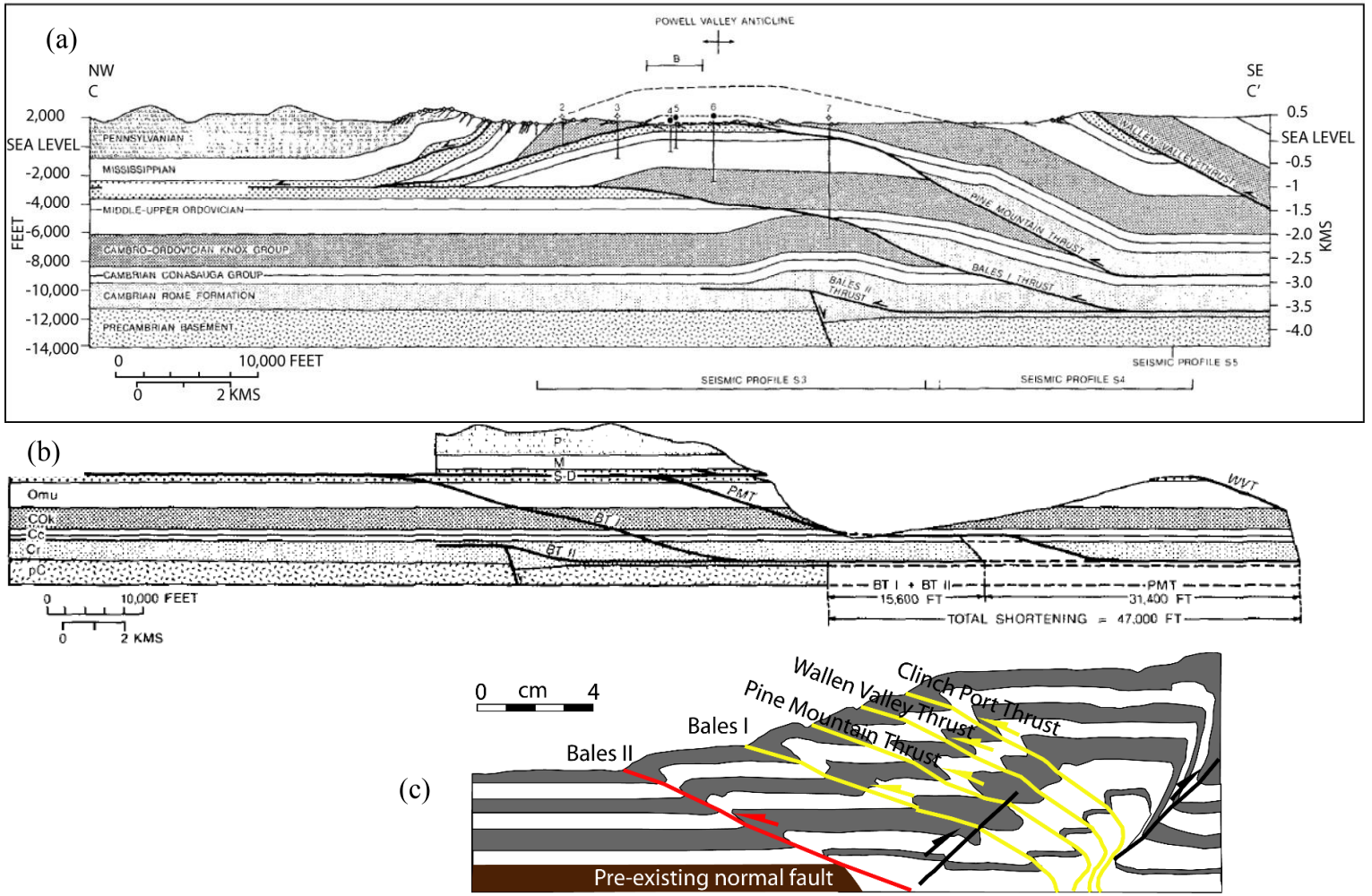

Figure 4.2 Section C-C' from the Figure 4.1 (a) Balanced cross-section; (b) restored section through the Martin Creek fenster [*Mitra*, 1988]; and (c) interpretation and comparison of the Pine Mountain thrust systems with the brittle detachement on the frontal ramp (model BDFR) section. 1-7 are well names mentioned in Figure 4.1.

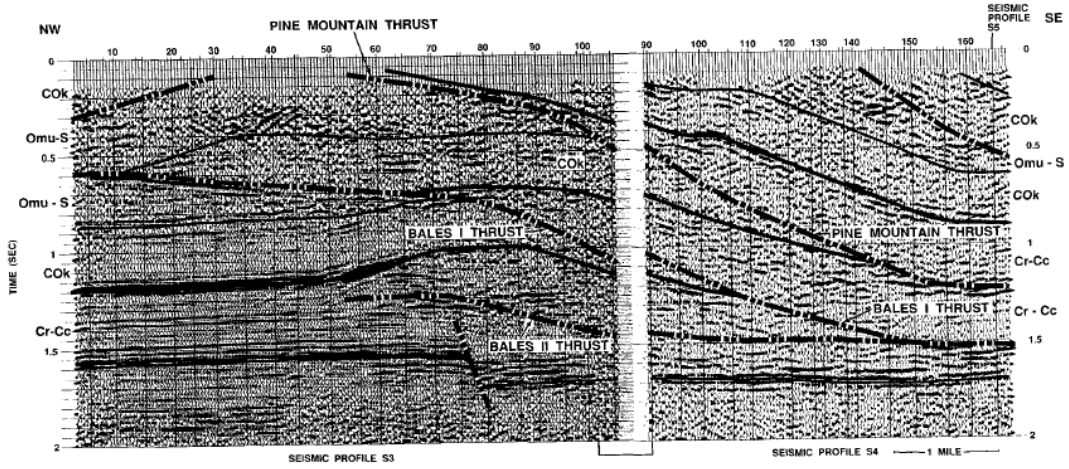

Figure 4.3 Interpreted (time-migrated) seismic profiles S3 and S4 along section C-C' in the Martin Creek fenster area (see Figure 4.1 for location) [*Mitra*, 1988].

The geometry and position of the forethrusts are controlled by the presence of the normal faults which is observed in the Bales I and Pine Mountain thrust sheets folded by the Bales II subthrust. Imbricate thrusts are translated in a piggyback sequence and rotated. Although the main objective of the current modeling approach is not to replicate the exact structural styles of Pine Mountain fold-thrust geometry and kinematics, however, the model BDFR explains the general geometry of the Pine Mountain thrust belts as controlled by the pre-existing normal fault. Usually, fold-thrust structures within the pre-existing normal fault are interpreted in a cross-section along the thrust dip. The experimental models suggest that the dip cross-sections with the pre-existing normal fault may look similar in general for different normal fault settings; however, when examined in three dimensions, different structures may form spatially and temporally in different ramp configurations.

4.2 The Western Alps thrust system

4.2.1 Field structures

The Alps is formed from the closure of the Ligurian-Piemontese oceanic domain that opened during the Jurassic period after the Permo-Triassic to Early Jurassic rifting [*Von Raumer et al.*, 1999; *Guillot et al.*, 2009]. Later the Alps thrust sheets were emplaced during the Late Cretaceous, and Tertiary compressional phases which were affected by a highly heterogeneous crust within the Liassic half-grabens inherited from the rifting stage. In some places this compressional deformation was strong enough to obscure the pre-compressional basin geometry. During late Cretaceous, flysch basins developed in the internal domains which suggest the onset of the closure of the oceanic area and

beginning of the continental collision. The deformation was highly variable between the rigid basement and the weak Jurassic sediments. The primary objective of the current study is to explain the natural structures with the help of experimental models. Therefore the stratigraphic detail in the Western Alps is not presented in this thesis and see *Debelmas and Kerckhove* [1980] and *Lemoine et al.* [1987] for stratigraphic detail.

Most of the structures that developed during the rifting stage exhibit larger displacements than pre-rift structures, and have played a vital role in the location of the thrust-fold belt in the Tertiary contraction. The Frontal Pennine thrust formed during the Tertiary contraction is the major tectonic boundary that separates different Mesozoic units and divides the external and internal tectonic domains [*Debelmas and Kerckhove*, 1980] (Figure 4.4).

4.2.2 The Jura thrust systems

In the Jura, the Sole thrust detached Mesozoic cover sediments along Triassic evaporites which created detachment folds and imbricate faults above an undeformed rigid basement. The Jura fold-thrust belt and Bresse basin is bounded by two sets of normal faults which dip to west. The dipping of the normal faults and the contraction direction are same (Figure 1.1c). Thus, they did not act as buttress to the cover sediments. The frontal termination of the Jura detachment lies close to the Bresse basin. It lies in the more forward position of the sub-Alpine thrust systems. *Enay* [1982] proposed that the emergent fontal thrust overstepped and truncated at the Bresse basin normal faults (Figure 4.4). In this orientation, these normal faults were unfavorable for reactivation during contraction. Nevertheless, their presence dropped the Triassic detachment to the west and prevented the activation of the detachment. So they control

the site of the emergent thrust front in the Jura area [*Butler*, 1989]. Similar detachment between the basement and cover sediment occurs in the sub-Alpine thrust systems as observed beneath the Jura. Geophysical studies show the basement top beneath Jura thrust systems dips towards eastwards until it reaches the buried leading edge of the external Belledonne massif which is the surface expression of a hanging wall anticline lying on the frontal Alpine basement thrust or Sole thrust.

4.2.3 The Western Alps Vercors Sub-Alpine thrust systems

In the west Vercors district, the frontal thrust ramp is nucleated on a pre-existing normal fault named as Faille de l'Iser dipping towards the oncoming thrust sheets. Two sets of normal faults formed the asymmetrical sloping graben (Figure 4.6). In this region, the Jura and sub-Alpine thrust belts converge and becomes narrow. In some places, normal faults are truncated by the later thrusts [*Butler et al.*, 2006]. The detachment occurs in Liassic shale between the cover sediment and the basement which is basement involved in places where the basement is uplifted (Figure 4.7). The simplified balanced and restored cross-sections though the Vercors sub-Alpine thrust belt show the location and geometry of the Alpine frontal thrust controlled by the pre-existing normal faults (Figure 4.5 & Figure 4.6). This result is confirmed by the seismic, surface, and stratigraphic data. Moreover, the backthrust displacement and location are also controlled by the normal fault. Regional uplifts are spread out in the Vercors area which can be related to the steeply dipping normal faults probably penetrating deeply into the crust before acquiring listric geometry which are generally difficult to invert by dip slip movements. Furthermore, there is no evidence of reactivation of the normal fault as inversion except in the deeper crust [*Butler*, 1989]. They form buttresses to

displacement on cover detachments and gently inclined basement faults. This decrease in displacement on the hanging-walls due to buttresses leads to the generation of layer parallel shortening, gentle to tight folds depending on the amount of contraction, back-folds, backthrust systems, and short cut thrust geometries.

4.2.4 Models representing the Jura and the Westerns Alps thrust systems

None of the current models can exactly replicate the Jura and western Alps thrust sheets because the pre-existing normal fault in the Jura is dipping away from the oncoming thrust front (normal faults dipping towards the contraction direction in all experiments). Basin had sloping full graben structure before contraction in the western Alps. However, the farther propgation of the frontal Alpine thrust could be related to the ductile detachment models. The offset frontal ramps models explain the general structures formed in the western Alps although all structures from both experiments and nature do not match or form. The ductile detachment on offset ramp model (Figure 4.8a) could explain the general Jura thrust belt deformation style. The major pre-existing normal faults in the Jura fold-thrust belt are far from the sub-Alpine thrusts which lie near to the Bresse basin (Figure 4.4) whereas, in the Chambery and Vercors area the pre-existing normal faults are close to the sub-Alpine thrust belt. The frontal fold-thrust belt of the Jura lies ahead west of the main sub-Alpine (Bornes) thrust systems. While in the Vercors area, they are continuous and become narrow. Due to the farther offset of the pre-existing normal faults that dips away from the contraction direction in the northwest and ductile detachment at the Jura area, the frontal Alpine basement thrust propagated farther in the Jura than in the Vercors. The curved transfer zone or relay ramp joins this thrust in Burger hills and Chambery areas as observed in

the models DDOFR and BDOFR (Figure 4.8a & Figure 4.8b). Molasse basins in the Annecy regions is wider and deeper which is formed by the displacement of the sub-Alpine and the Jura thrust systems. Similar molasse basin was developed in the ductile detachment on the offset ramp experiment, model DDOFR (Figure 4.8a & Figure 4.8c). However, no major backthrust formed in the Jura as was observed in the model DDOFR.

Vercors subalpine thrust detaches in the Liassic shale, which resembles the brittle detachment on offset ramp configuration (model BDOFR). Foreland verging duplexes imbricate thrust sheets were formed and the frontal ramp was located by the pre-existing normal faults (Figure 4.6 & Figure 4.7). This model also explains the large scale backthrust in the Dome de la Mure massif (Figure 4.6).

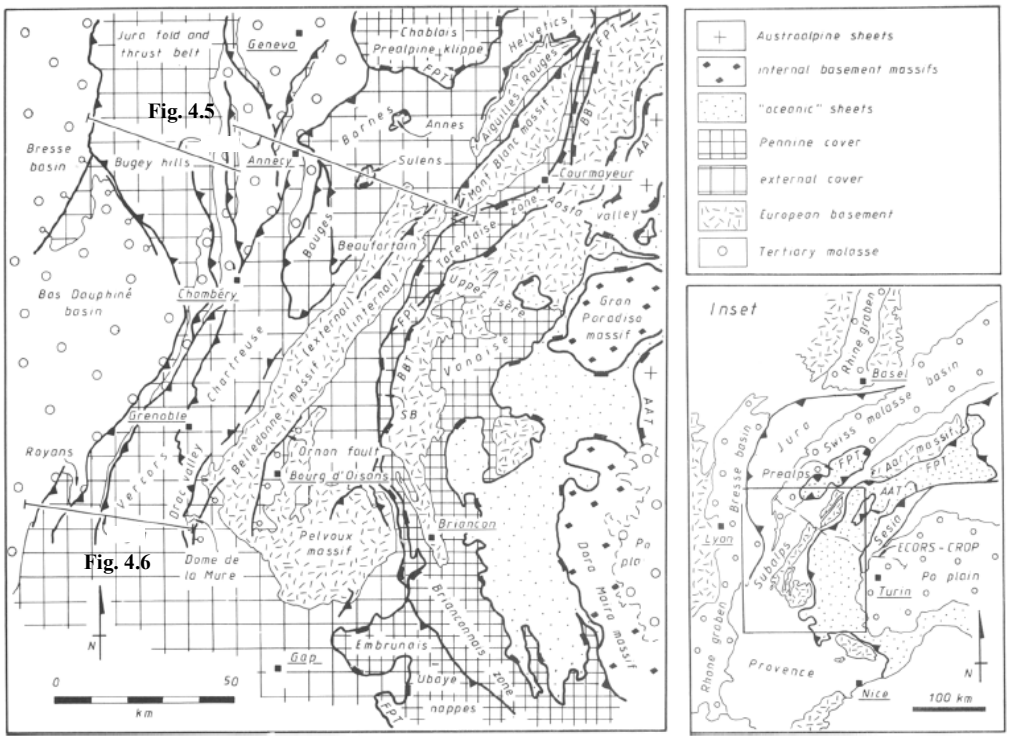

Figure 4.4 Simplified tectonic map of the NW Alps showing the main structural units and locations of the cross-sections (Figure 4.5 & Figure 4.6) FPT = Frontal Pennine thrust, BBT = Basal Brianconnais thrust, SB = SubBrianconnais zone, AAT-Austro-alpine thrust. The inset shows the location of the study area [*Butler*, 1989].

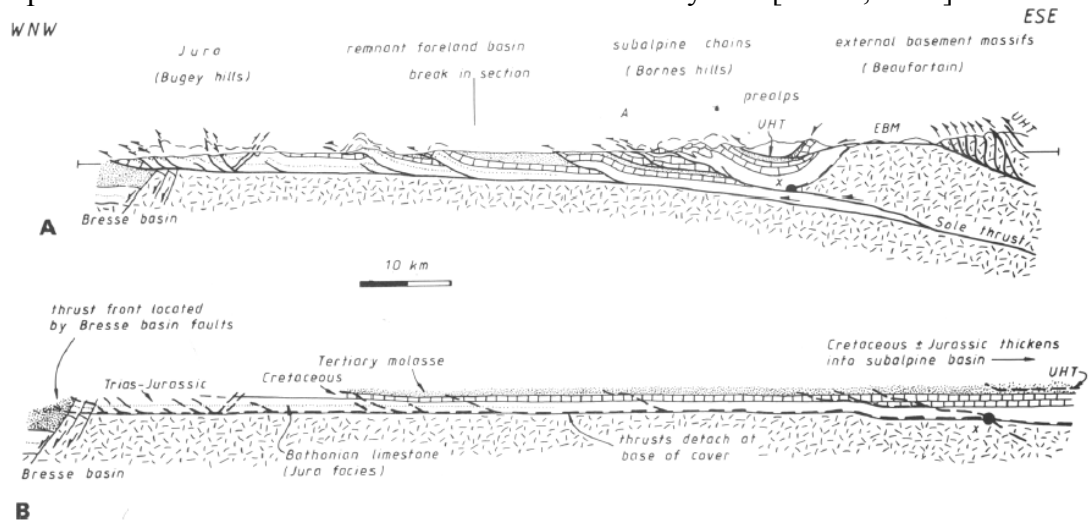

Figure 4.5 (a) Simplified balanced; (b) restored cross-section through the Jura and sub-Alpine chains along the Bornes transect (see Figure 4.4 for location). The frontal thrust overstepped and truncated pre-existing normal fault Bresse basin faults. UHT = Ultrahelvetic thrust, EBM = External Belledonne massif, A = Annecy town [*Butler*, 1989].

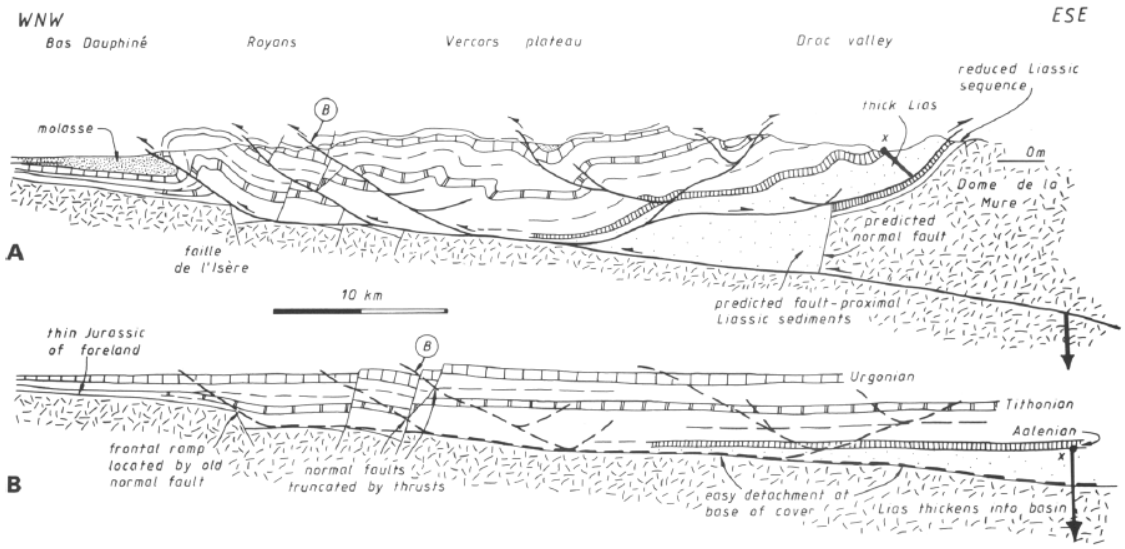

Figure 4.6 (a) Simplified balanced; (b) restored cross-section through the Vercors subalpine along the Bornes transect (see Figure 4.5 for location). B = Cole de la Bataille area 5 km south of line [*Butler*, 1989].

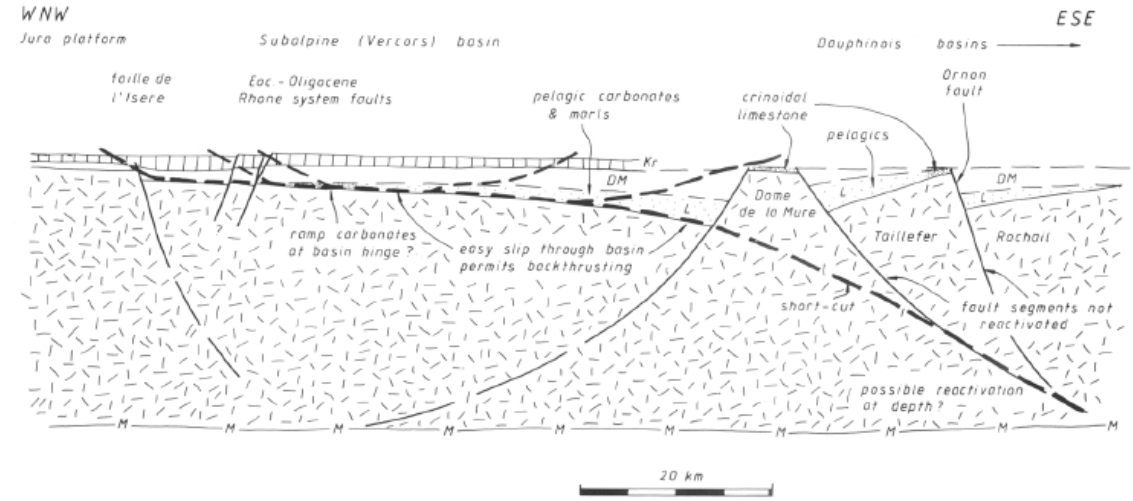

Figure 4.7 Simplified true scale restored crustal section through the Vercors and neighboring districts showing the distribution of Mesozoic basins and the predicted geometry of the bounding normal faults. The dashed line shows the future position of the Alpine Sole thrust system [*Butler*, 1989].

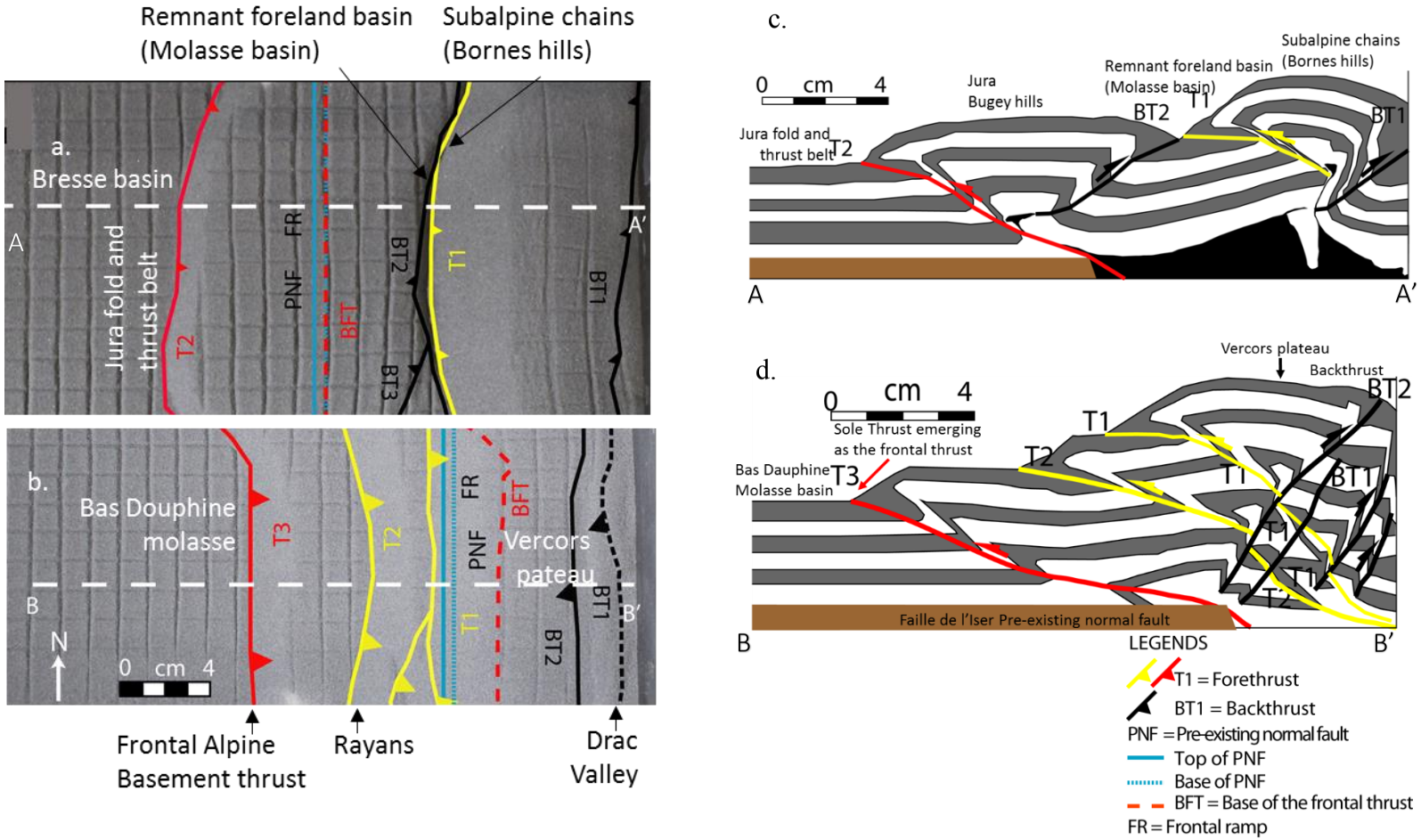

Figure 4.8 Partial top photo after 9 cm shortening in offset ramp experiments showing fault interpretation of the Western Alps. (a) Ductile detachment (model DDOFR) shows the general structures like the Jura fold-thrust belt; (b) brittle detachment (model BDOFR) explains the Vercors sub-Alpine thrust. (c) Cross-section A-A' and (d) cross-section B-B'.

4.3 Northeastern Salt Range-Potwar fold-thrust belts

4.3.1 Field structures

The Salt Range-Potwar fold-thrust belt is developed south of the Himalayas because of a continuous collision between India and Eurasia plates [*Baker et al.*, 1988; *Jaumé and Lillie*, 1988]. This collision caused southward-verging fold-thrust deformation in this region above a basal detachment within the Neoproterozoic Salt Range Formation[*Lillie et al.*, 1987]. There are three main zones of tectonic deformations across the Salt Range-Potwar Plateau: from north to south, these are the Northern Potwar deformation zone (NPDZ), the Soan syncline, and the Salt Range (Figure 4.9).

The progressively propagating southward thrust system has brought allochthonous Cambrian to Quaternary sedimentary units to the surface and overthrusted over Quaternary rocks of the autochthonous foreland basin [*Crawford*, 1974; *Seeber and Armbruster*, 1979]. The South Potwar Basin is hydrocarbon prolific because of the well-developed anticlinal structures. In this region the rocks range in age from Precambrian to Recent and comprise four major unconformity-bounded sequences [*Jaswal et al.*, 1997]. They are (1) Precambrian crystalline rocks of the Indian craton, (2) Neoproterozoic evaporite (Salt Range Formation), (3) Cambrian-Eocene (Carapace strata), and (4) Miocene-recent molasses sediments (Rawalpindi and Siwalik groups).

The Precambrian crystalline basement that is cut by normal faults from Neoproterozoic rifting dips gently to the north at 1° in the Salt Range and 3°-4°in the Potwar. Thrust ramp is situated above a north-dipping basement normal fault that has a displacement of

1 km, decreasing toward the east which is well imaged on seismic profiles [*Lillie et al.*, 1987; *Baker et al.*, 1988] (Figure 4.10).

The NPDZ consists of a complex stack of imbricated thrust faults. *Jaswal et al.* [1997] state that the NPDZ is a passive roof duplex with a roof thrust located at the base of the Murree Formation and a sole thrust at the top of the basement. The transition between the South Potwar Basin and the NPDZ is separated by the triangle zone located beneath the Khari Murat forethrust and the Soan backthrust [*Baker et al.*, 1988; *Jaswal et al.*, 1997]. The Potwar Basin, an autochthonous foreland basin is bounded by the Salt Range thrust in the south and by the Soan backthrust or Dhurnal Fault in the north. It subsequently became a piggyback basin. Complex detachment folds, hinterland and foreland-verging thrusts faults are observed in the eastern part of the basin whereas, few deformation features are observed in the western part [*Lillie et al.*, 1987; *Baker et al.*, 1988]. The emergent Salt Range Thrust places the Salt Range Formation and Cambrian-Eocene Carapace rocks onto recent sediments [*Gee*, 1980; *Yeats et al.*, 1984]. This Salt Range Thrust becomes blind in the east Potwar. *Grelaud et al.* [2002] used the seismic data to forward model the present compressional structures in the Salt Range and Potwar Plateau. They showed the pop-up structures and fault bend fold developed above the pre-existing normal faults (Figure 4.10 & Figure 4.11).

Qayyum [1991] suggests an east-dipping transverse fault or lateral ramp cutting cover sediment but not a basement at the east end of the Salt Range province. This lateral ramp produced telescoping deformation style and a lateral culmination, apparent as Chambal Ridge. In contrary rigid translation deformtion style controlled by the frontal ramp is observed in the Salt Range [*Faisal and Dixon*, 2015].

4.3.2 Comparison to the experimental models

Normal faults also influence the location of other thrust faults in the area. Brittle detachment on the frontal ramp, model BDFR, explains the NPDZ that has imbricated thrusts and duplex structures with an incipient of backthrust at the hinterland. The Soan syncline and Salt Range Thrust structures can be explained by the ductile detachment on the frontal ramp experiment, model DDFR (Figure 4.12b). The Eastern Potwar Plateau deformation zone is likely similar to a ductile detachment on the lateral ramp experiment, model DDLR (Figure 4.13). As observed in the East Potwar Plateau, the frontal thrust in the lateral ramp ductile detachment model propagated farther on the back end of the lateral ramp (Figure 4.13). In this region, broader pop-up structures and gentler folds developed in the eastern Potwar Plateau than in the central and western Potwar Plateau. Narrower tight small detachment folds, pop-ups, and thrusts are developed in the central and western side as observed in the model (Figure 4.13).

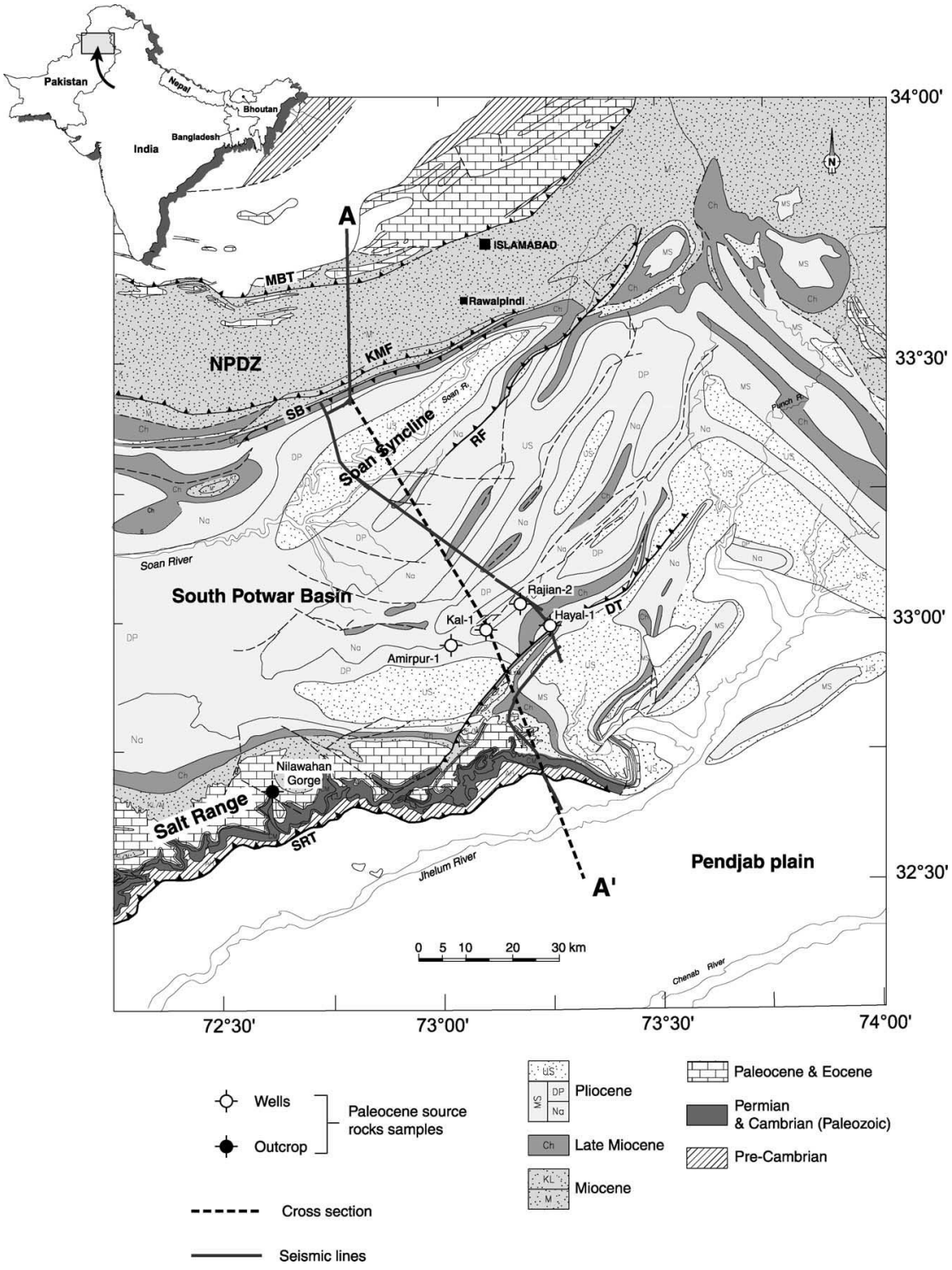

Figure 4.9 Geological map of the eastern Salt Range and Potwar Plateau. A-A' is seismic transect. MBT = Main Boundary Thrust, KMF = Khari Murat fault, DT = Domeli Thrust, SRT = Salt Range Thrust, RF = Riwat Fault, SB = Soan Backthrust (Adapted from *Grelaud et al.* [2002])

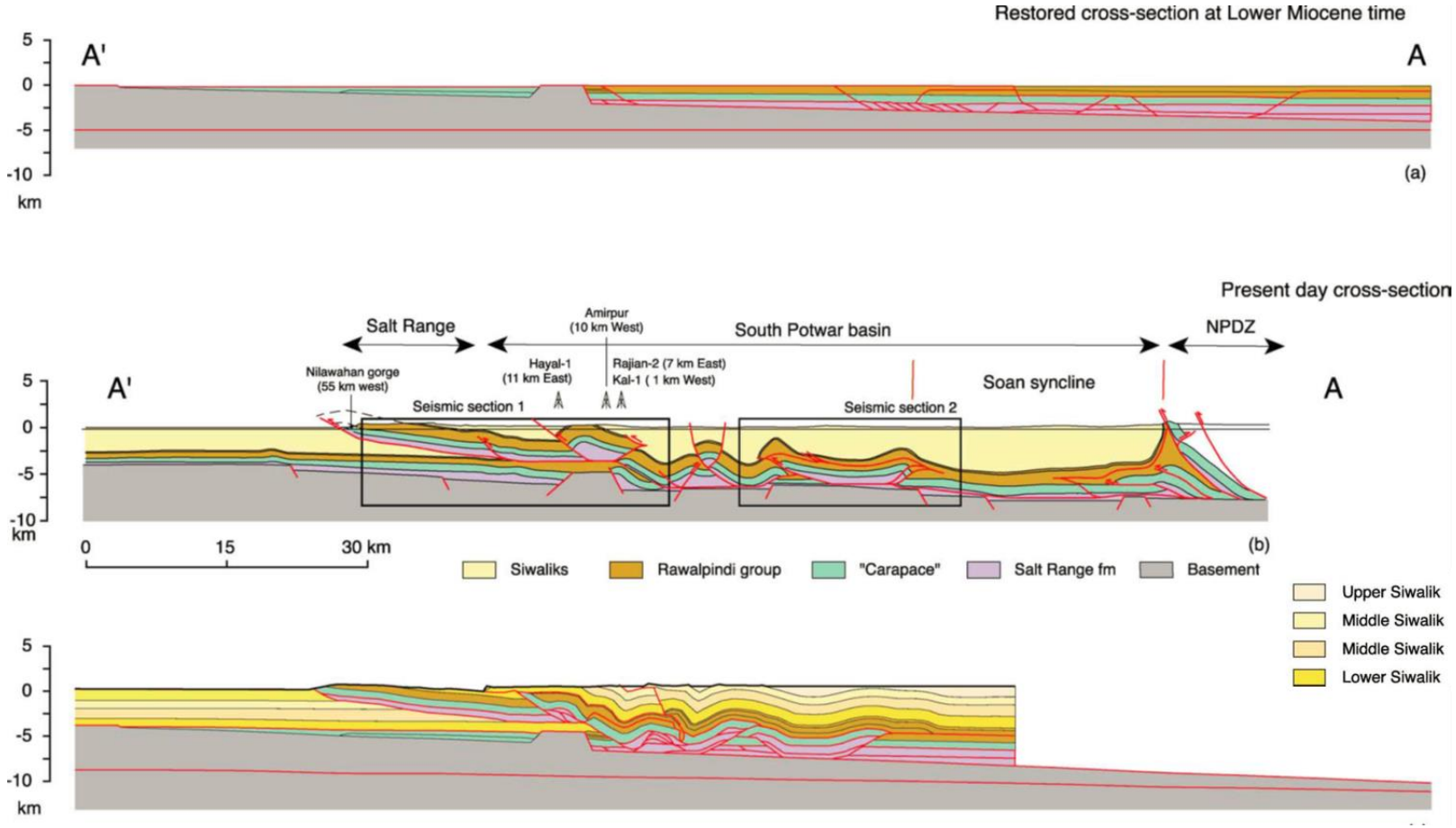

Figure 4.10 Initial and final geometry from the THRUSTPACK model of the Salt Range and Potwar Plateau compared with the corresponding interpreted cross-section. (a) Initial stage model (Oligocene) with predefined tectonic units corresponding to the cross-section prior to folding; (b) Depth-converted cross-section using seismic data (see Figure 4.9 & Figure 4.11); (c) Result of the forward modeling [*Grelaud et al.*, 2002].

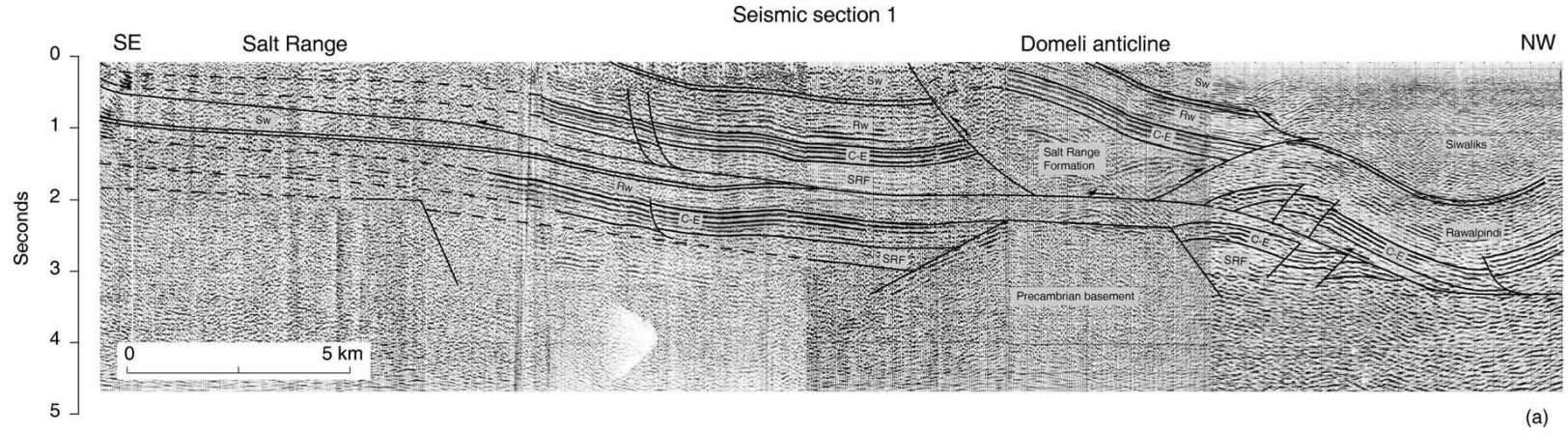

Figure 4.11 Interpreted seismic lines into the cross section (see Figure 4.10). (a) Line drawing showing the varying shape of the Salt Range thrust and north dipping normal fault responsible for creating the thrust ramp. C-E = Cambrian to Eocene carbonates [*Grelaud et al.*, 2002].

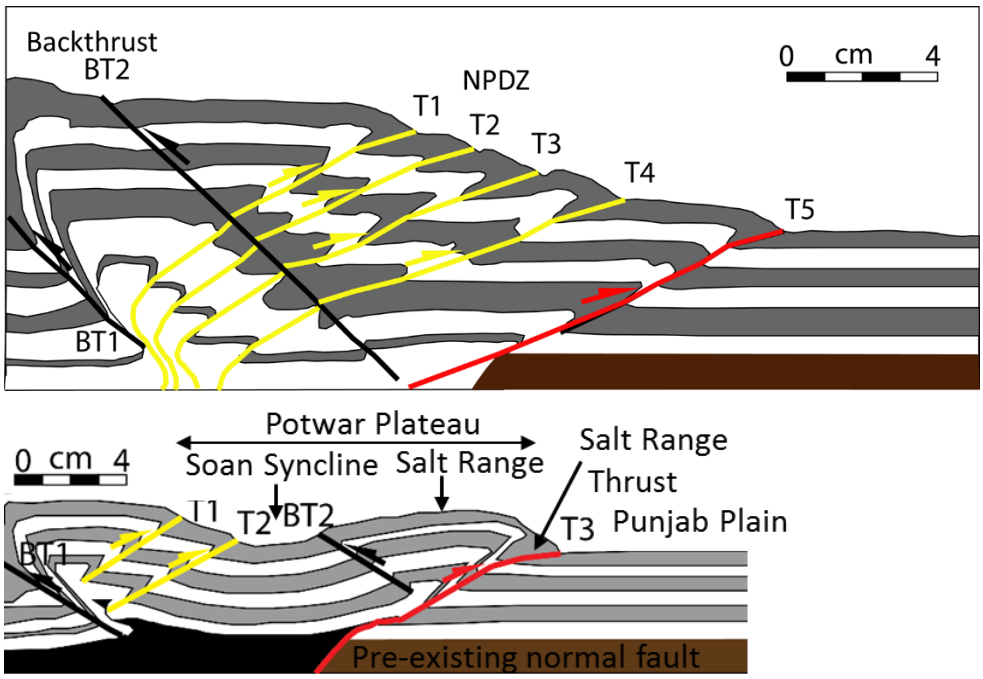

Figure 4.12 Model explaining tectonics evolution of tectonic zones of Potwar Salt Range Province. (a) Brittle detachment on the frontal ramp experiment, model BDFR showing NPDZ (Northern Potwar Deformation Zone) (see Figure 3.1); (b) ductile detachment on the frontal ramp experiment, model DDFR (see Figure 3.4) explains the formation of Soan Syncline, Salt Range, Salt Range Thrust, and Punjab Plain.

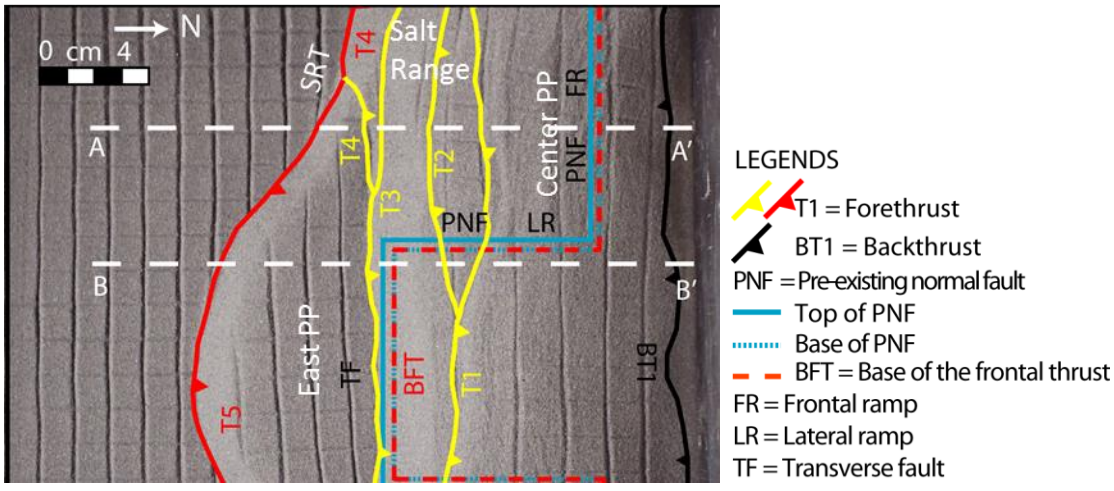

Figure 4.13 Ductile detachment on a frontal ramp bounded by a vertical lateral ramp experiment, model DDLR that includes structures in the eastern and western Potwar Plateau. PP = Potwar Plateau, SRT = Salt Range Thrust.

Conclusions

1. The analog models for both brittle and ductile detachments suggests that pre-existing normal faults play an important role in determining the geometry and kinematics of fold-thrust belts. The normal faults influence the location and orientations of later formed thrusts, rather than the sequence of fault propagation. In some instances, the presence of the normal faults changes the fault spacing.

2. The normal fault acts as a buttress and influences the position of the base of the thrust fault. For brittle detachments, the base off the thrust is usually a small distance from the normal fault, whereas for ductile detachments, the base is either at or very close to the normal fault. Frontal fault dips are greater for ductile detachments than for brittle detachments.

3. Favorably oriented frontal thrusts along the normal fault propagate faster and farther when the frontal thrust uses the normal fault as a ramp.

4. Brittle detachment result in a slower propagation of the deformation front to the normal fault, the formation of a larger number of faults, and a steeper wedge, whereas ductile detachments result in faster propagation of the front to the normal fault and a gentler taper.

5. A linear frontal normal fault ramp results in a linear frontal thrust. Normal faults oriented obliquely to the contraction direction result in oblique frontal thrusts, whereas normal faults with offsets result in thrust fronts with transverse or oblique

segments. Backthrusts formed during the formation of the structures also have geometries and orientations that follow the geometry of the normal faults.

6. Curved normal faults result in curved frontal thrusts. The obliquity of the transfer fault is greater for a ductile detachment. For frontal ramps separated by two lateral ramps, two transfer zones develop in both brittle and ductile models.
7. In summary, the effect of the pre-existing normal faults on the thrust-fold geometry depends on the relative distance between the normal fault and the forethrust positions, detachment type, and the geometry of the normal fault.

References

Bahroudi, A., and H. Koyi (2003), Effect of spatial distribution of Hormuz salt on deformation style in the Zagros fold and thrust belt: an analogue modelling approach, *Journal of the Geological Society*, *160*(5), 719-733.

Baker, D. M., R. J. Lillie, R. S. Yeats, G. D. Johnson, M. Yousuf, and A. S. H. Zamin (1988), Development of the Himalayan frontal thrust zone: Salt Range, Pakistan, *Geology*, *16*(1), 3-7.

Bose, S., and S. Mitra (2009), Deformation along oblique and lateral ramps in listric normal faults: Insights from experimental models, *AAPG Bulletin*, *93*(4), 431-451.

Butler, R. W. (1989), The influence of pre-existing basin structure on thrust system evolution in the Western Alps, *Geological Society, London, Special Publications*, *44*(1), 105-122.

Butler, R. W., E. Tavarnelli, and M. Grasso (2006), Structural inheritance in mountain belts: an Alpine–Apennine perspective, *Journal of Structural Geology*, *28*(11), 1893-1908.

Cobbold, P., E. Rossello, and B. Vendeville (1989), Some experiments on interacting sedimentation and deformation above salt horizons, *Bulletin de la Société Géologique de France*(3), 453-460.

Costa, E., and B. Vendeville (2002), Experimental insights on the geometry and kinematics of fold-and-thrust belts above weak, viscous evaporitic décollement, *Journal of Structural Geology*, *24*(11), 1729-1739.

Cotton, J. T., and H. A. Koyi (2000), Modeling of thrust fronts above ductile and frictional detachments: Application to structures in the Salt Range and Potwar Plateau, Pakistan, *Geological Society of America Bulletin*, *112*(3), 351-363.

Crawford, A. (1974), The Indus suture line, the Himalaya, Tibet and Gondwanaland, *Geological Magazine*, *111*(05), 369-383.

Davis, D. M., and T. Engelder (1985), The role of salt in fold-and-thrust belts, *Tectonophysics*, *119*(1), 67-88.

Debelmas, J., and C. Kerckhove (1980), Les Alpes francoitaliennes *Geologie Alpine*, *56*, 21-58.

Dixon, J. M., and D. A. Spratt (2004), Deformation at Lateral Ramps and Tear Faults Centrifuge Models and Examples from the Canadian Rocky Mountain Foothills, In: McClay, K.R. (Ed.), *Thrust Tectonics and Hydrocarbon Systems, American Association of Petroleum Geologists Memoir*, *82*, 239-258.

Enay, R. (1982), Notice explicative de la feuille Saint-Rambert-en Bugey à 1/50 000, *Bureau de Recherches Géologiques et Minières*.

Faisal, S., and J. M. Dixon (2015), Physical analog (centrifuge) model investigation of contrasting structural styles in the Salt Range and Potwar Plateau, northern Pakistan, *Journal of Structural Geology*, *77*, 277-292.

Gee, E. (1980), Salt Range series geological maps: Directorate of Overseas Surveys, *United Kingdom, for the Government of Pakistan and Pakistan Geological Survey, scale*, *1*(50,000), 6.

Glennie, K., and P. Boegner (1981), Sole pit inversion tectonics, in *Petroleum geology of the continental shelf of North-West Europe*, edited, pp. 110-120, Institute of Petroleum London.

Grelaud, S., W. Sassi, D. F. de Lamotte, T. Jaswal, and F. Roure (2002), Kinematics of eastern Salt Range and South Potwar basin (Pakistan): a new scenario, *Marine and Petroleum Geology*, *19*(9), 1127-1139.

Groshong, R., and D. Rodgers (1978), Left-lateral strike-slip fault model, *Structural Style of the Arbuckle Region. Geological Society of America, South Central Section*, *1*, 2-7.

Guillot, S., K. Hattori, P. Agard, S. Schwartz, and O. Vidal (2009), Exhumation processes in oceanic and continental subduction contexts: a review, in *Subduction Zone Geodynamics*, edited, pp. 175-205, Springer.

Horsfield, W. (1977), An experimental approach to basement-controlled faulting, *Geologie en Mijnbouw*, *56*(4), 363-370.

Hubbert, M. K. (1937), Theory of scale models as applied to the study of geologic structures, *Geological Society of America Bulletin*, *48*(10), 1459-1520.

Jaswal, T. M., R. J. Lillie, and R. D. Lawrence (1997), Structure and evolution of the northern Potwar deformed zone, Pakistan, *AAPG Bulletin*, *81*(2), 308-328.

Jaumé, S. C., and R. J. Lillie (1988), Mechanics of the Salt Range-Potwar Plateau, Pakistan: A fold-and-thrust belt underlain by evaporites, *Tectonics*, *7*(1), 57-71.

Karama, P. (2014), Analog modelling of salt structure, 100 pp, The University of Oklahoma, Norman, OK.

Koyi, H. A., and N. S. Mancktelow (2001), *Tectonic modeling: A Volume in Honor of Hans Ramberg*, Geological Society of America.

Lemoine, M., P. Tricart, and G. Boillot (1987), Ultramafic and gabbroic ocean floor of the Ligurian Tethys (Alps, Corsica, Apennines): In search of a genetic imodel, *Geology*, *15*(7), 622-625.

Letouzey, J. (1990), *Petroleum and tectonics in mobile belts: proceedings of the 4th IFP Exploration and Production Research Conference, held in Bordeaux, November 14-18, 1988*, Editions Technip.

Letouzey, J., B. Colletta, R. Vially, and J. C. Chermette (1995), Evolution of salt-related structures in compressional settings, *AAPG Memoir*, *65*, 41-60.

Lillie, R. J., G. D. Johnson, M. Yousuf, A. S. H. Zamin, and R. S. Yeats (1987), Structural development within the Himalayan foreland fold-and-thrust belt of Pakistan, *Sedimentary Basins and Basin-forming Mechanisms, Memoirs of the Canadian Society of Petroleum Geologists*, *12*, 379-392.

Lowell, J. D. (1970), Antithetic Faults in Upthrusting: GEOLOGICAL NOTES, *AAPG Bulletin*, *54*(10), 1946-1950.

McClay, K. (1989), Analogue models of inversion tectonics, *Geological Society, London, Special Publications*, *44*(1), 41-59.

Mitra, S. (1986a), Duplex structures and imbricate thrust systems: geometry, structural position, and hydrocarbon potential, *AAPG Bulletin*, *70*(9), 1087-1112.

Mitra, S. (1988), Three-dimensional geometry and kinematic evolution of the Pine Mountain thrust system, southern Appalachians, *Geological Society of America Bulletin*, *100*(1), 72-95.

Mitra, S. (1993), Geometry and kinematic evolution of inversion structures, *AAPG Bulletin*, *77*(7), 1159-1191.

Mitra, S., and Q. T. Islam (1994), Experimental (clay) models of inversion structures, *Tectonophysics*, *230*(3-4), 211-222.

Nilforoushan, F., H. A. Koyi, J. O. Swantesson, and C. J. Talbot (2008), Effect of basal friction on surface and volumetric strain in models of convergent settings measured by laser scanner, *Journal of Structural Geology*, *30*(3), 366-379.

Qayyum, M. (1991), Crustal shortening and tectonic evolution of the Salt Range in Northwest Himalaya, Pakistan.

Reches, Z. (1978), Analysis of faulting in three-dimensional strain field, *Tectonophysics*, *47*(1-2), 109-129.

Sanford, A. R. (1959), Analytical and experimental study of simple geologic structures, *Geological Society of America Bulletin*, *70*(1), 19-52.

Sassi, W., B. Colletta, P. Balé, and T. Paquereau (1993), Modelling of structural complexity in sedimentary basins: the role of pre-existing faults in thrust tectonics, *Tectonophysics*, *226*(1-4), 97-112.

Schreurs, G., S. J. Buiter, D. Boutelier, G. Corti, E. Costa, A. R. Cruden, J. Daniel, S. Hoth, H. A. Koyi, and N. Kukowski (2006), Analogue benchmarks of shortening and extension experiments, *Geological Society of London, Special Publication*, *253*, 1.

Seeber, L., and J. Armbruster (1979), Seismicity of the Hazara arc in northern Pakistan: decollement vs. basement faulting, *Geodynamics of Pakistan*, *131*, 142.

Tavarnelli, E. (1996), The effects of pre-existing normal faults on thrust ramp development: an example from the Northern Apennines, Italy, *Geologische Rundschau*, *85*(2), 363-371.

Tsuneishi, Y. (1978), Geological and experimental studies on mechanism of block faulting *Bulletin of the Earthquake Research Institute*, *53*.

Von Raumer, J., J. Abrecht, F. Bussy, B. Lombardo, R. Ménot, and U. Schaltegger (1999), The Paleozoic metamorphic evolution of the Alpine external massifs, *Schweizerische Mineralogische und Petrographische Mitteilungen*, *79*, 5-22.

Weijermars, R., and H. Schmeling (1986), Scaling of Newtonian and non-Newtonian fluid dynamics without inertia for quantitative modelling of rock flow due to gravity (including the concept of rheological similarity), *Physics of the Earth and Planetary Interiors*, *43*(4), 316-330.

Withjack, M. O., J. Olson, and E. Peterson (1990), Experimental models of extensional forced folds (1), *AAPG Bulletin*, *74*(7), 1038-1054.

Yeats, R. S., S. H. Khan, and M. Akhtar (1984), Late quaternary deformation of the Salt Range of Pakistan, *Geological Society of America Bulletin*, *95*(8), 958-966.